UNIVERSITY OF OKLAHOMA

GRADUATE COLLEGE

MODELLING, ADDITIVE MANUFACTURING, AND TESTING OF KNITTED MATERIALS

A THESIS

SUBMITTED TO THE GRADUATE FACULTY

in partial fulfillment of the requirements for the

Degree of

MASTER OF SCIENCE

By

ALEXANDRIA ROSE THOMAS
Norman, Oklahoma
2024

Downloaded from SHAREOK. Persistent Handle URL: https://hdl.handle.net/11244/340340

MODELLING, ADDITIVE MANUFACTURING,
AND TESTING OF KNITTED MATERIALS

A THESIS APPROVED FOR THE
SCHOOL OF AEROSPACE AND MECHANICAL ENGINEERING

BY THE COMMITTEE CONSISTING OF

Dr. Philip Scott Harvey Jr., Chair

Dr. Yingtao Liu

Dr. Christopher Dalton

© Copyright by ALEXANDRIA ROSE THOMAS 2024
All Rights Reserved.

Acknowledgements

I would like to express my deepest gratitude to my advisor, Dr. Harvey, whose constant guidance and support have been essential to this project. From guiding my initial steps into research to encouraging my novel interest into knitting and 3D printing that sparked this thesis, I am so grateful for your mentorship. I also extend many thanks to my defense committee, who generously provided their insight and expertise.

Special thanks to parents and their unwavering support and encouragement. Even if you weren't quite sure what I was ranting about when I came home to tell you about my work, your unwavering belief in me and willingness to lend an ear have always been a source of strength.

To my roommates and friends who I was able to drag along to social dance events and garage shows, I am grateful for your friendship and camaraderie. Despite the crushed toes, our time together provided me much-needed moments of relaxation, enabling me to keep focused on my studies amid the challenges of academic life.

This material is based upon work supported by the National Science Foundation under Grant No. NSF-CMMI-1943917. Any opinions, findings and conclusions or recommendations expressed in this material do not necessarily reflect the views of NSF.

Thank you,

Rose

Contents

Acknowledgments **iv**

Contents **v**

List of Figures **vii**

List of Tables **x**

Abstract **xi**

1 Introduction **1**
1.1 Overview 1
1.2 Original Inspirations 1
1.3 Literature Review 2
1.3.1 Overview of Knitting 2
1.3.2 Novel Applications of Knitting 4
1.3.3 Modelling of Knitting 5
1.3.4 Additive Manufacturing Techniques 6
1.3.5 Additive Manufacturing of Knit Materials 7
1.4 Summary 9

2 Specimen Design and Fabrication **10**
2.1 Overview 10
2.2 Geometry 10
2.3 CAD Modelling 13
2.4 3D Printing Procedure 15
2.4.1 Failures and Defects 17
2.5 Summary 18

3 Experimental Setup and Testing Protocol **20**
3.1 Overview 20
3.2 Tensile Extension Testing 20
3.2.1 Methods 20
3.2.2 Testing Protocol 22
3.2.3 Tests Conducted 23

3.3 Cyclic Testing . . . 23
3.3.1 Methods . . . 23
3.3.2 Testing Protocol . . . 25
3.3.3 Tests Conducted . . . 26
3.4 Summary . . . 26

4 Results and Discussion **27**
4.1 Overview . . . 27
4.2 Base Specimen . . . 27
4.2.1 Baseline Testing . . . 27
4.2.2 Tests Performed with Spacers . . . 34
4.3 Non-Base Specimen . . . 36
4.3.1 Thick and Thin Specimens . . . 36
4.3.2 Narrow Specimen . . . 37
4.3.3 Short Specimens . . . 39
4.4 Specimens with Print Defects . . . 39
4.4.1 Testing in the Course Direction . . . 40
4.4.2 Testing in the Wale Direction . . . 41
4.4.3 Testing with a Short Specimen . . . 41
4.5 Cyclic Tests . . . 42
4.5.1 Testing in the Course Direction . . . 42
4.5.2 Testing in the Wale Direction . . . 43
4.6 Normalized Comparisons . . . 44
4.7 Summary . . . 45

5 Summary, Conclusions, and Future Work **49**
5.1 Summary and Conclusions . . . 49
5.2 Future Work . . . 51

Bibliography **54**

A Print Settings **56**

List of Figures

1.1 "Front stitches and back stitches: simulations of (a) the front stitch, (b) jersey knit made from all front stitches, (c) the back stitch and (d) jersey knit made from all back stitches and (e) representative colors to indicate segments of front stitches and back stitches (color online only). (Simulations (a)–(d) were produced using Shima Seiki SDS-ONE Apex 3 Software.)" Source: Amanatides et al. (2022, Figure 1) 3
1.2 "Front and back stitch patterns represented on using a helicoid-based modeling system (described in References 18-20), demonstrating the three-dimensionality of stitches in vertical (top) and horizontal (bottom) front-to-back stitch transitions." Source: (Amanatides et al., 2022, Figure 2) 3
1.3 "Characteristic edge rolling behavior of jersey knit fabric, as seen from the front stitch side and the back stitch side." Source: Amanatides et al. (2022, Figure 5) 4

2.1 The large-scale knitting that used for reference for the models 11
2.2 The plan view of the geometry of the unit stitch 12
2.3 The 3D model of the stitch unit 14
2.4 The 3D model of an alternate version of the stitch unit 14
2.5 The basic stockinette assembly 15
2.6 Prusa's slicing software with the base sample, with the print details . . . 16
2.7 The (a) base specimen, (b) thin specimen, (c) thick specimen, (d) short specimen, and (e) narrow specimen 17
2.8 The first layer of the base specimen 18
2.9 Printed base specimens without any defects (a) and with defects (b,c) . . 18

3.1 The displacement each cycle of the Instron testing underwent 21
3.2 The models of the 3D printed (a) rig to the Instron machine and (b) hangers used to hook the specimens on. All dimensions shown are in mm 22
3.3 (a) The model of the 3D printed spacers, and (b) the spacers threaded onto the rod. All dimensions shown are in mm 22
3.4 The set-up of (a) Specimen SC1, (b) Specimen BW1, and (c) Specimen BC1 25

4.1 The load-extension curves for base specimen loaded in the course direction: (a) Specimen BC1 and (b) Specimen BC2 29
4.2 The load-extension curves for Specimen BC1, with a close-up of the initial loading 30
4.3 The load-extension curves for Specimen BC1, with stiffness noted . . . 30
4.4 The broken Specimen BC2 after undergoing tensile extension in the course direction 31
4.5 The load-extension curves for base specimen loaded in the wale direction: (a) Specimen BW1 and (b) Specimen BW2 32
4.6 The load-extension curves for Specimen BW2, with a close-up of the initial loading 33
4.7 The load-extension curves for Specimen BW2, with energy at each cycle plotted as dots on the right axis 33
4.8 The load-extension curves for two base specimen loaded in the course (Specimen BC1) and wale (Specimen BW2) directions 34
4.9 The load-extension curve for a base specimen with spacers (Specimen BC3) loaded in the course direction 35
4.10 The base specimen with spacers (Specimen BC3) after undergoing tensile extension in the course direction 35
4.11 The load-extension curve for a base specimen with spacers (Specimen BW3) loaded in the wale direction 36
4.12 The broken base specimen with spacers (Specimen BW3) after undergoing tensile extension in the wale direction 37
4.13 The load-extension curve for the thick specimen (Specimen TC1) loaded in the course direction. Specimen BC1's load-extension curve is shown in grey 37
4.14 The load-extension curve for narrow specimen loaded in the course direction: (a) Specimen NC1 and (b) Specimen NC2. Specimen BC1's load-extension curve is shown in grey 38
4.15 The load-extension curve for a short specimen (Specimen SC1) loaded in the course direction. Specimen BC1's load-extension curve is shown in grey 39
4.16 Specimen SC1 after undergoing tensile extension in the course direction 40
4.17 The load-extension curve for defective Specimen BC4 loaded in the course direction. Specimen BC1's load-extension curve is shown in grey 40
4.18 The load-extension curve for defective Specimen BW4 loaded in the wale direction. Specimen BW2's load-extension curve is shown in grey 41
4.19 The load-extension curve for defective Specimen SC2 loaded in the course direction. Specimen BC1's load-extension curve is shown in grey 42
4.20 The load-extension curve for defective Specimen BC5 loaded cyclically in the course direction. A close-up is presented in the upper left-hand corner with a limited number of cycles shown 43

4.21 The energy for defective Specimen BC5 loaded cyclically in the course direction 43
4.22 The load-extension curve for defective Specimen BW5 loaded cyclically in the wale direction 44
4.23 The normalized load-extension curves for tests with extension in the (a) course direction and (b) wale direction 46

5.1 The anisotropic behavior base specimen while loosely hanging with the print-bed side (a) up and (b) down 52
5.2 The self-actuating behavior of a base specimen when in compression from the (a) wale direction and (b) course direction 52
5.3 The behavior of the specimen when it is rolled in the (a) wale direction and (b) course direction 53

A.1 Layer Settings 56
A.2 Infill Settings 57
A.3 Advanced Settings 57
A.4 Speed Settings 58

List of Tables

2.1 The parameters used to formulate the unit stitch's geometry 12
2.2 The specimens printed 16

3.1 The tests performed 24

4.1 The ultimate load and extension of each specimen, compared to the normalized ultimate values. The course specimens are compared in the first half, the wale in the second 47

Abstract

Knitting is a centuries-old textile fabrication technique utilizing a method of "interlooping," where loops are pulled through each other until the final product is created. It has the ability to easily stretch, which makes it perfect for form-fitting items such as sweaters, socks, and hats. In addition, certain patterns curl in on themselves, which can allow for unique self-actuating properties. Though this property may be a nuisance for someone creating a textile that is intended to be flat, it can be manipulated by engineers. While this manipulation has been proven with fabric samples, it has not been applied to more rigid materials, such as thermoplastics commonly used in 3D printing. This thesis will further explore fabricating knit specimens with 3D printing. The geometry of a knit stitch is established, then used to create a 3D model that can be replicated to form a specimen of a stockinette pattern that can then be 3D printed without the need for support material. Several baseline specimens were fabricated using PLA with a consumer-grade 3D printer. Additional, several specimens with altered "yarn" diameters or altered number of repetitions of the stitch unit were fabricated to further characterize the behavior of a additively manufactured knit specimen. Additional parametric variation was provided by altering boundary conditions to allow or disallow contraction. The 15 printed specimens were then tested in tensile extension and cyclic patterns with a universal testing machine. The results are then presented and compared with load-extension graphs. The load-extension graphs of each specimen were compared, and it was noted that specimens exhibited energy dissipation and had anisotropic behavior.

Chapter 1

Introduction

1.1 Overview

This chapter explores the fundamental concepts of knitting and its novel applications, as well as defining the fundamental concepts and practices of additive manufacturing through a literature review. Finally, it examines the existing literature on models of knitted materials and how additive manufacturing can be used to fabricate knit specimens.

1.2 Original Inspirations

The inspiration for this topic came from Kamien (2022), a presentation discussing the geometry of knitting and details the unique, self-actuating properties that knitted structures have. This discussion prompted the question: are these properties exclusive the traditionally manufactured, flexible material, or can they be leveraged with a more rigid material – such as an additively manufactured plastic? Though the concept of using additive manufacturing to create knitted materials is not unique, its current use is primarily in the fashion industry. Several studies have show that fused deposition modelling (FDM) printers can successfully create flexible knit structures, but the majority of them do not conduct scientific testing or analysis (Chatterjee and Ghosh, 2020; Beecroft, 2016, 2019; Xiao and Kan, 2022; Melnikova et al., 2014; Uysal and Stubbs, 2019).

1.3 Literature Review

Much of the analysis on knitted materials focuses on either using fabric knits with novel applications, the modelling process of knitting, or the basic process of 3D printing, or additively manufacturing, a knitted structure. An in-depth look at each of these subjects will be taken in the following sections.

1.3.1 Overview of Knitting

First, an in-depth look must be taken at what knitting is and how it is created. Knitting is the process of making textiles through "interlooping," or putting loops of yarn through other loops until a textile is formed. Knitting specifically uses needles, which manipulate the yarn to to draw a new loop through the existing ones (Spencer, 2001; Leong et al., 2000). A textile that is knitted is typically referred to as having a "wale" and a "course" direction, as seen in Fig. 1.1. It is easiest to think of the wale direction as the columns of the textile, and the course direction as the rows of loops.

There are two methods that the loops can be pulled through each other. The new loop can be pulled through the front of the existing loop, which results in the existing loop being pushed to the back of the fabric. This is called a "back stitch" and is the most basic form of hand knitting. The new loop can also be pulled through the back of the existing loop, which results in the existing loop being pushed to the front of the fabric. This is referred to as a "front stitch," or a "purl" stitch (Amanatides et al., 2022). These two stitches are seen in Fig. 1.2. With hand knitting, since the product is flipped at the end of every row, if the basic "knit" stitch is used, the final product's pattern switches between front stitches and back stitches over each course. This is called a "garter" stitch (Wadekar et al., 2020).

Many patterns require both front and back stitches to be used. The most common, which is also typically what knitting machines produce, is a "stockinette" or "jersey"

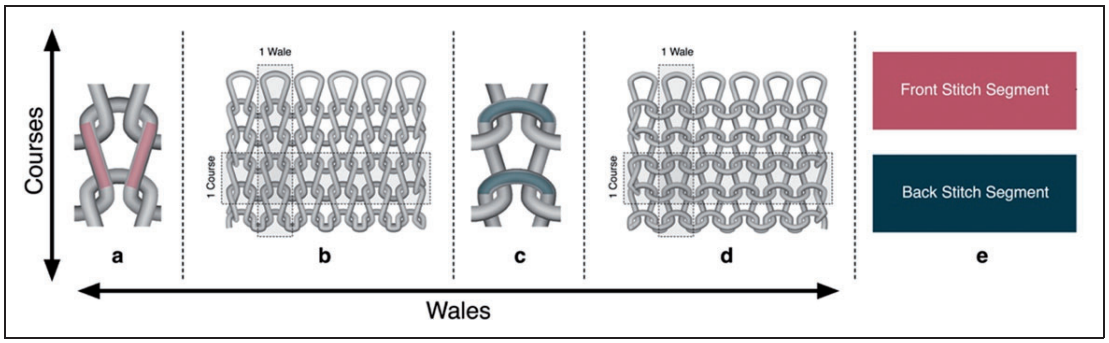

Figure 1.1: "Front stitches and back stitches: simulations of (a) the front stitch, (b) jersey knit made from all front stitches, (c) the back stitch and (d) jersey knit made from all back stitches and (e) representative colors to indicate segments of front stitches and back stitches (color online only). (Simulations (a)–(d) were produced using Shima Seiki SDS-ONE Apex 3 Software.)" Source: Amanatides et al. (2022, Figure 1)

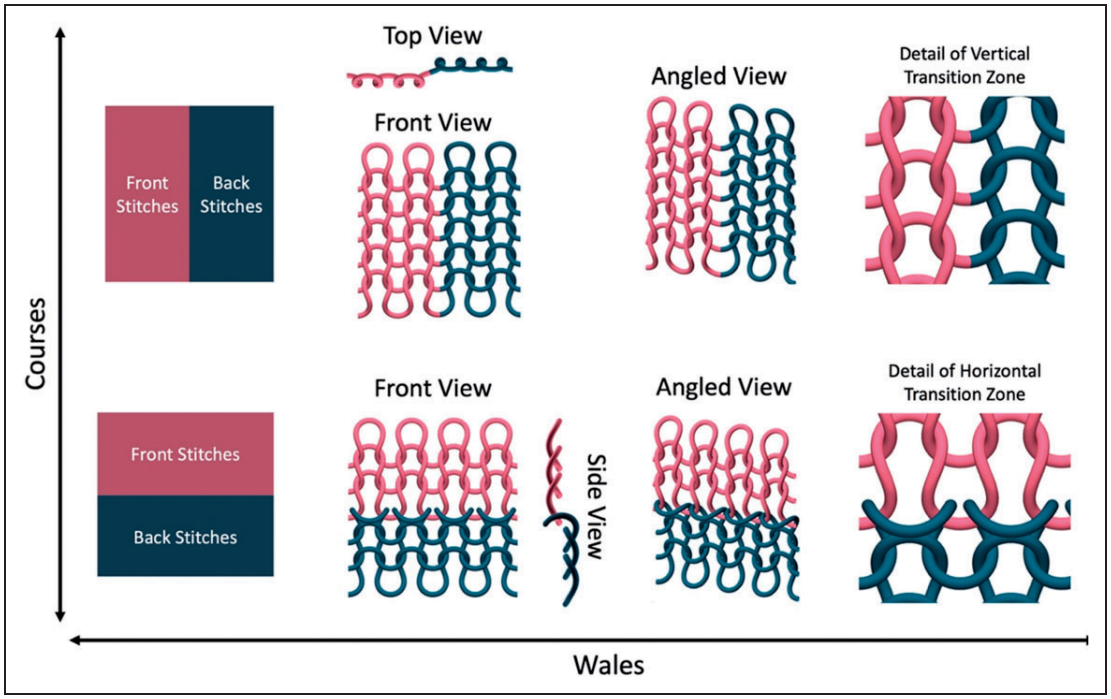

Figure 1.2: "Front and back stitch patterns represented on using a helicoid-based modeling system (described in References 18-20), demonstrating the three-dimensionality of stitches in vertical (top) and horizontal (bottom) front-to-back stitch transitions." Source: (Amanatides et al., 2022, Figure 2)

knit. Stockinette patterns use only front or only back stitches. These are often used for fabrics where a smooth surface is preferred, such as socks or a scarf. They, as well as other patterns that use large amounts of one stitch across several rows of course, often

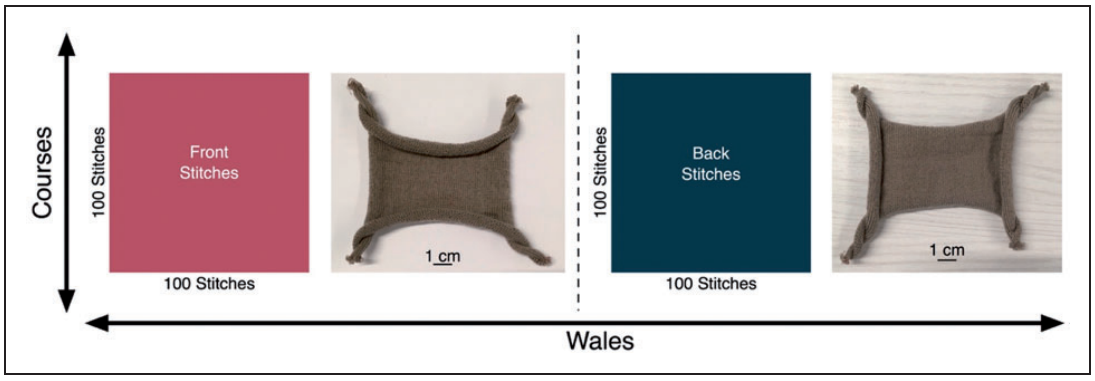

Figure 1.3: "Characteristic edge rolling behavior of jersey knit fabric, as seen from the front stitch side and the back stitch side." Source: Amanatides et al. (2022, Figure 5)

display a unique property – the edges roll up, as seen in Fig. 1.3. This is often annoying to knitters who had planned on a flat, rectangular scarf and now have a curled tube, but this property can be manipulated to an engineer's benefit, as discussed in the following section.

1.3.2 Novel Applications of Knitting

With its unique flexibility and curling, there are many engineering applications that knit materials can be used for. One such example uses the concept of "tensegrity," which is a system that achieves static equilibrium by distributing discontinuous compressive elements within a network of tensile elements (Gupta et al., 2020). To create a structure, a knitting machine fabricates a large, flexible shell out of knitting. Rigid struts are added to key points, which results in a self-supporting, domed structure. Many similar dome-like structures currently require complex, rigid, curved parts to be transported, or complex parts to be manufactured on-site. However, by using flexible knit and tensegrity, unique structures can be designed and their parts can be easily manufactured, transported, and assembled.

Another novel application is using liquid crystal elastomer (LCE) to create actuators. LCE is a polymer known for its ability to undergo large, reversible deformations. One

of the most common fabrication techniques is additive manufacturing. By fabricated a yarn with LCE and knitting it, an actuator can be created that has in-plane and out-of-plane deformation abilities (Sun et al., 2023).

While both applications successfully create a final product using knitting, neither explore the full possibilities of creating a final product with additive manufacturing. By manufacturing a rigid knit, the necessity of struts is eliminated in the tensengrity structural design and LCEs could simply be 3D print the knit design, instead of 3D printing the LCEs and then knitting it. This would simplify both fabrication processes.

1.3.3 Modelling of Knitting

As mentioned in Section 1.2, knitting is know to have rolling, self-actuating properties that can be manipulated into forming specific shapes (Kamien, 2022). These properties can also be modeled so that the behavior of a textile can be predicted with certain patterns of front and back stitches (Amanatides et al., 2022).

Additionally, there have also been several attempts to use computational and mathematical models to try to characterize knitting. One used "helicoid scaffolds" to characterize knit (back stitch), purl (front stitch), rib fabric (where the front and back stitches are alternated in each wale), and garter fabric.Wadekar et al. (2020, 2021) optimized the curvature to ensure the geometry was accurate, and they were able to generate models with random patterns of knit and purl stitches with various scaling factors for the height of one stitch. Some 3D models are formulated specifically to aid in design complex and accurate 3D models for machine knitting (Liu et al., 2020) .

While those methods of modelling provide an in-depth look at how knitting functions, a model for 3D printing does not have to be that complex. A model for 3D printing only must get the basic geometry correct, and it must stay simple enough to be successfully printed. Ding et al. (2021) accurately models a stockinette pattern, which is simple enough to model in standard Computer Aided Drafting (CAD) software and

being able to be additively manufactured. The geometry was supported with a mathematical model, but the edges of the specimen were left unconnected. This model seems to simulate a textile material with multiple different pieces of yarn, instead of a specimen made out of one unbroken strand. The results that Ding et al. (2021) found are further discussed in Section 1.3.5.

1.3.4 Additive Manufacturing Techniques

3D printing, also known as additive manufacturing, refers to a variety of techniques used to quickly fabricate items by adding material in layers. The general additive manufacturing process starts with creating a model in a CAD software, exporting to STL file, slicing the STL file and generating GCODE so that it can be transferred to the 3D printer, printing it, post-processing, and finally being able to using it for its intended application (Gibson et al., 2020). Since the parts are created layer-by-layer, complex geometries that are difficult to create using traditional subtracting manufacturing are easy with additive manufacturing. Internal features are simple to fabricate, as are organic and intricate geometries. Additionally, it is generally faster to create a specimen with additive manufacturing than it is with traditional manufacturing.

The first additive manufacturing method to be patented was stereolithography (SLA). This technique cures resin with a UV light or laser in layers until the final structure is complete (Wickramasinghe et al., 2020). Another common method is powder-bed fusion or selective laser sintering (SLS). This technique also uses a laser, this time curing layers of powder resting on a bed (Wickramasinghe et al., 2020). One of the most common methods of additive manufacturing is fused deposition modelling, or FDM. To manufacture something with this method, layers of thermoplastic filaments are melted and deposited onto a heated bed through a heated nozzle (Wickramasinghe et al., 2020). Since this technique is very common in industry, academia, and hobby printing, and thus is widely accessible, FDM will be used to fabricate the specimens

in this thesis. Additionally, many studies have concluded that FDM printing, ideally with supports for more complex garter patterns, is the one of the better methods to create knitted specimens with additive manufacturing though SLS may also be useful (Chatterjee and Ghosh, 2020; Melnikova et al., 2014; Beecroft, 2016).

1.3.5 Additive Manufacturing of Knit Materials

The concept of fabricating a textile product, specifically one that has the same pattern as knit, is not a new one. In 2008, Campbell (2008) proposed using inkjet printing, a form of additive manufacturing where drops of ink are deposited and cured to form a structure, to produce unique textiles. They looked at building surface texture on already-existing fabric, and printing novel structures similar to knit and woven fabrics. Inkjet printing is typically used to fabricate 2-dimensional products, and thus the support necessary to print something that truly resembled a knit fabric is not possible.

Much of the literature on 3D printed knit focuses on fabricating something wearable. The main goals for these studies are to understand the unique characteristics of textiles, and their relationship with structural features, and to investigate best practices and methods for fabricating 3D printed textiles. For wearable specimens, the inherent anisotrophy that comes with additive manufacturing is desirable, as yarn is anisotropic so the final product of an anisotropic 3D print is more similar to how traditional fabrics than something with an isotrophic material (Chatterjee and Ghosh, 2020). Melnikova et al. (2014) experimented with using SLS and FDM to print knitted specimens with polylactic acid (PLA), as well as woven and lace patterns. It is noted that though SLS did not require support structures, FDM was able to fabricate a specimen that was more desirable due to its flexibility and similarity to a traditionally manufactured knit specimen. This study serves as proof of concept, showing that a knit pattern could be manufactured with additive manufacturing techniques. There is no mention of measures taken to characterize the behavior of the fabricated specimens, either qualitatively or

quantitatively.

Beecroft (2016) also provides some proof of concept for FDM printing of knit materials using a flexible nylon filament. While they do provide some results on the behavior, it is mostly qualitative. They show that the specimens do not snap upon being handled and can be easily manipulated by hand. Beecroft (2019) follows up on this study by re-fabricating specimens using SLS and the same nylon powder. Though the testing is more thorough, it only discusses the approximate distance that the prints can be compressed, extended, stretched, and folded by hand. Measurements appear to be taken with a simple ruler.

As mentioned in Section 1.3.3, Ding et al. (2021) model a knit pattern that is sufficient for 3D printing and then prints it using a recycled, flexible onyx filament. This article focuses on qualitative testing, as one of the main goals is to characterize the filament after it has been through the recycling process. The knitted specimens were tested in tensile extension. They tested two specimens – one being stretched in the wale direction and one in the course. They modeled the specimens such that they had the same dimensions, so for the specimen being stretched in the wale direction it had 24 stitches in the course direction and 4 in the wale, while the specimen being stretched in the course direction had 6 stitches in the course direction and 15 in the wale. It was found that both specimens exhibited curling behavior, and that the specimen tested in the wale direction was able to withstand significantly less extension and load than the specimen stretched in the course direction. The reason for failure appeared to be a combination of unravelling, as the edges were not connected to each other, and fractures in the specimen.

1.4 Summary

This chapter discussed what knitting is, its novel applications, what additive manufacturing is, and how additive manufacturing can be used to produce knitted materials. In its most simple form, knitting is a series of loops that have been strung through each other. With certain patterns of knitting, a self-actuating curling occurs. These patterns were studied by Kamien (2022) and Amanatides et al. (2022). There are also many unique, novel applications for knitting, though most explorations into these rely on traditionally manufactured fabric knitting (Gupta et al., 2020; Sun et al., 2023). Several studies have detailed complex methods to modelling knitting, and many have evaluated using additive manufacturing to fabricate knitted materials. However, many of the models of knitting are too complex for 3D printing, and much of the literature looking into 3D printed knit does not qualitatively or quantitatively evaluate the properties of the knit, as their goals align more with ensuring proof of concept for wearable textiles. In Chapter 2 the geometry this thesis uses to model knitting and the model itself will be discussed. The fabrication and experimental set-up are detailed in Chapter 3. Chapter 4 discusses the results of the experimental tests. Finally, Chapter 5 summarizes and concludes the thesis.

Chapter 2

Specimen Design and Fabrication

2.1 Overview

As discussed in the Chapter 1, one of the most important parts of producing an additively manufactured item is creating an accurate model. This chapter discusses the literature used as a basis for the model, the modelling process, and the additive manufacturing process used to fabricate the specimens.

2.2 Geometry

The basic geometry of knit stitches was studied from the models shown in Beecroft (2016, 2019) and Amanatides et al. (2022). Additionally, a model of a large-scale knit fabrics (see Fig. 2.1) was also produced in-house. This model included sections of garter stitch as well as stockinette. It was clear that the most important part of the model would have to the be correctly modelling the base geometry of the lattice structure. The first step of creating this model is creating a basic unit, or "stitch." The unit is made of a semi-circle linearly connected to two arcs. The two lower arcs serve as connection points so that it may be repeated in the course direction to form the final specimen. Methods for repetition in the wale direction will be touched on in Section 2.3.

To create the basic stitch used in the FDM prints and testing, the parameters seen in Table 2.1 were established. The "base" parameters of radius r and diameter d could



Figure 2.1: The large-scale knitting that used for reference for the models

be varied to alter the weave's tightness or thread size, respectively. The radius, r, was set to be 5 mm, and stayed constant through the tests conducted. The thread's diameter was altered from 4/3 mm to 2 mm through tests. Fig. 2.2 shows the basic 2D geometry for each stitch.

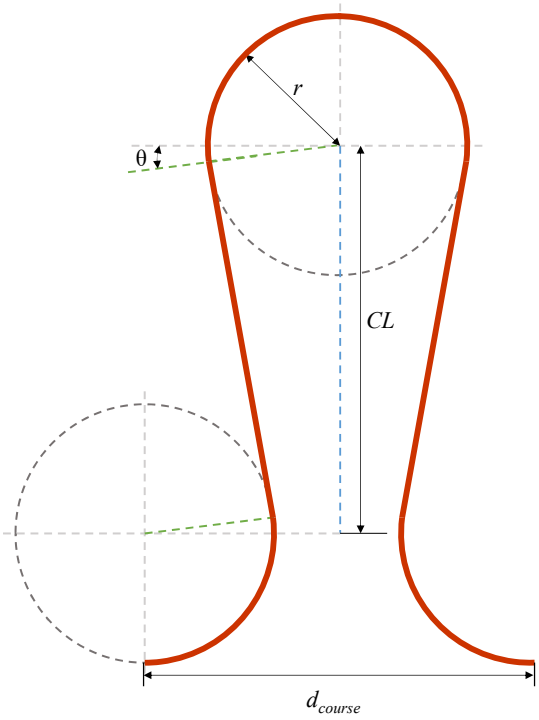

Figure 2.2: The plan view of the geometry of the unit stitch

Table 2.1: The parameters used to formulate the unit stitch's geometry

Variable	Use	Relation	Base Values
d	"thread" diameter	user-defined	5/3 mm
r	radius of arcs	user-defined	5 mm
CL	centerline length of stitch	$3 \times r$	15 mm
θ	angle that the line connecting the two arcs is offset from the center	$\tan^{-1}\left(\frac{CL}{r/2}\right)$ $-\cos^{-1}\left(\frac{r}{[CL^2+(r/2)^2]^{1/2}}\right)$	9.7°
d_{wale}	distance between stitch units	$(0.5 \times CL) + r$	15 mm
d_{course}	distance between stitch units	$3 \times r$	12.5 mm
h	height of the spline connecting the two arcs	$d + 0.5 \times r$	4.167

2.3 CAD Modelling

Fusion 360 was chosen to create the knit models. Using the geometry previously formulated as a base, a 3D drawing was created. This drawing could be extruded with the "pipe" tool so that it was 3D and had a consistent diameter. However, it was discovered that ensuring the unit could be replicated in the course direction was more difficult that previously assumed. In fabric knitting, the fibers lie on top of each other, naturally forming a bulge in the center of a stitch unit. However, since this model will be 3D printed and it cannot have intersecting components. There are two methods to fix this: (1) a bulge is added to the model or (2) the elevation of the arcs is altered so that one side is raised. To accommodate this change, additional parameters were added. For the first method, h refers to the height that the center point of the line connecting the two arcs met, seen in Fig. 2.3. To ensure that all these connections were smooth, splines were used to connect the two arcs. The height h was set to be $d + (0.5 \times r)$. For the second method, h refers the change in elevation, as seen in Fig. 2.4. Ultimately, though the second method could be used to model both front and back stitches stitches, it would be very difficult to print using FDM without substantial support material; therefore, the first method was chosen to create the final specimen's assemblies.

After the stitch unit was finalized, it could be brought into an assembly and duplicated in the course and wale directions. The final assembly is seen in Fig. 2.5. The loops at the edge were added such that all the courses were connected, so that it was made out of one piece of continuous "yarn". This also avoids the issue of unravelling that Ding et al. (2021) confronted in their studies. Additionally, and notably, there was no support material necessary to print this design.

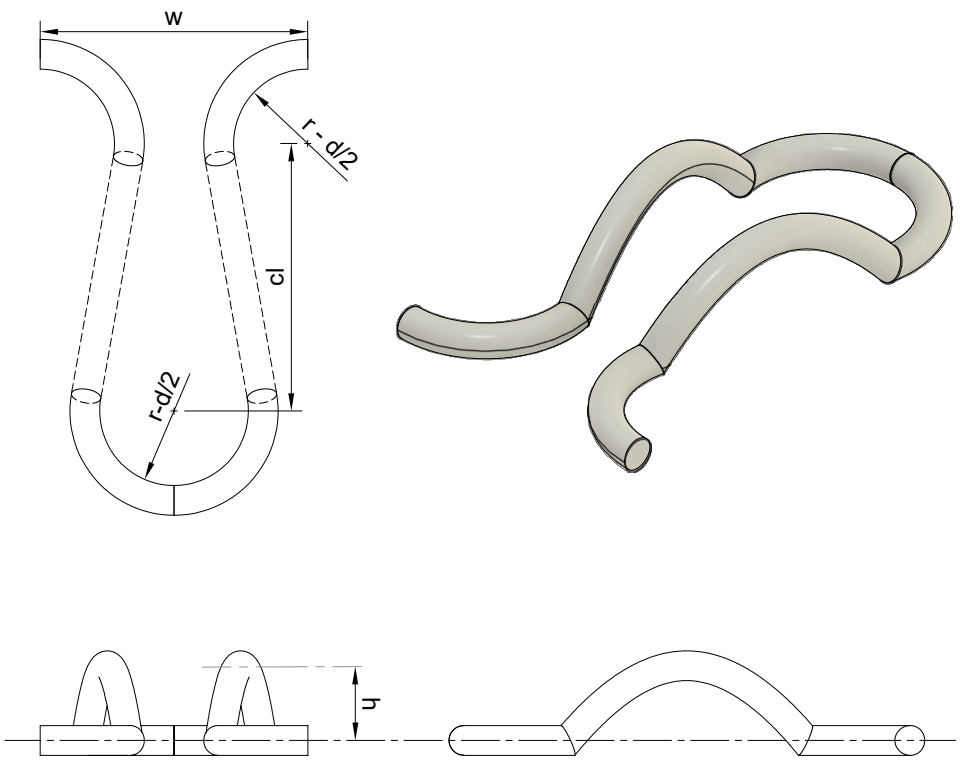

Figure 2.3: The 3D model of the stitch unit

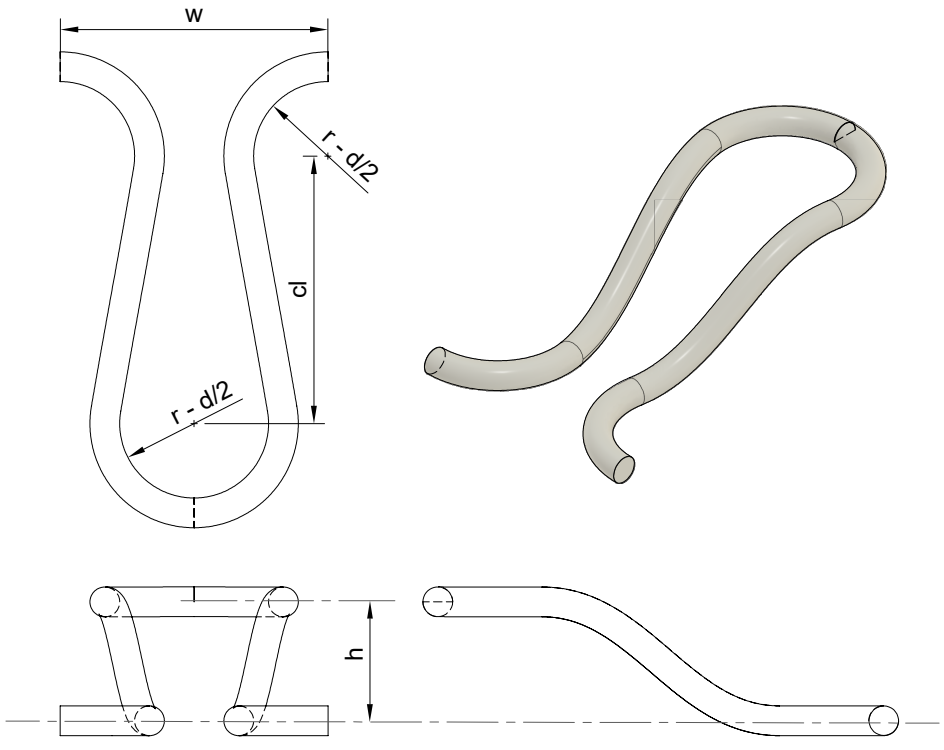

Figure 2.4: The 3D model of an alternate version of the stitch unit

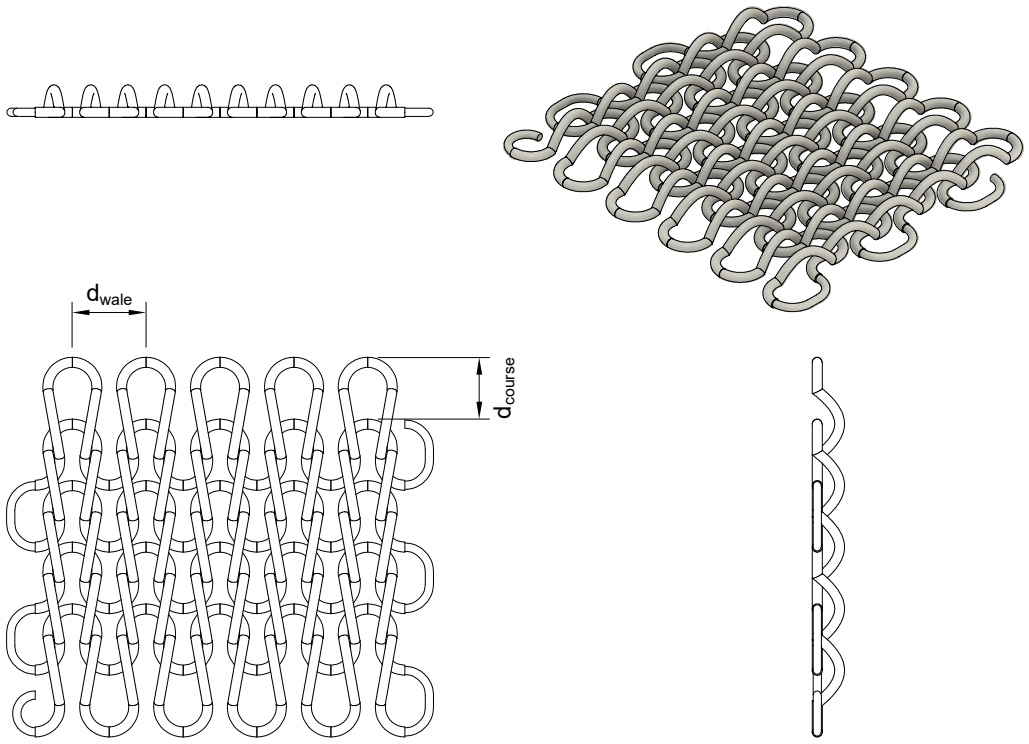

Figure 2.5: The basic stockinette assembly

2.4 3D Printing Procedure

To print the samples, they were exported to STL files. A consumer-grade Prusa i3 MK3S was used to print these samples, and the PrusaSlicer software was used to export the STL file to GCode. The settings were set to "0.30mm DRAFT." A layer height of 0.3 mm was used, with an infill of 100%. The material used was Polymaker Polylite PLA (Porter et al., 2019). Figure 2.6 shows the base sample within the slicing software. The complete splicer settings are given in Appendix A.

The "base" specimen had the parameters as defined in Table 2.1 and 11 units in each direction. In addition to base specimen, four versions with altered geometry were printed and tested, as described in Table 2.2. They are also shown in Fig. 2.7 The first two altered the diameter of the "yarn," or variable d. The *Thin Yarn* specimen dropped

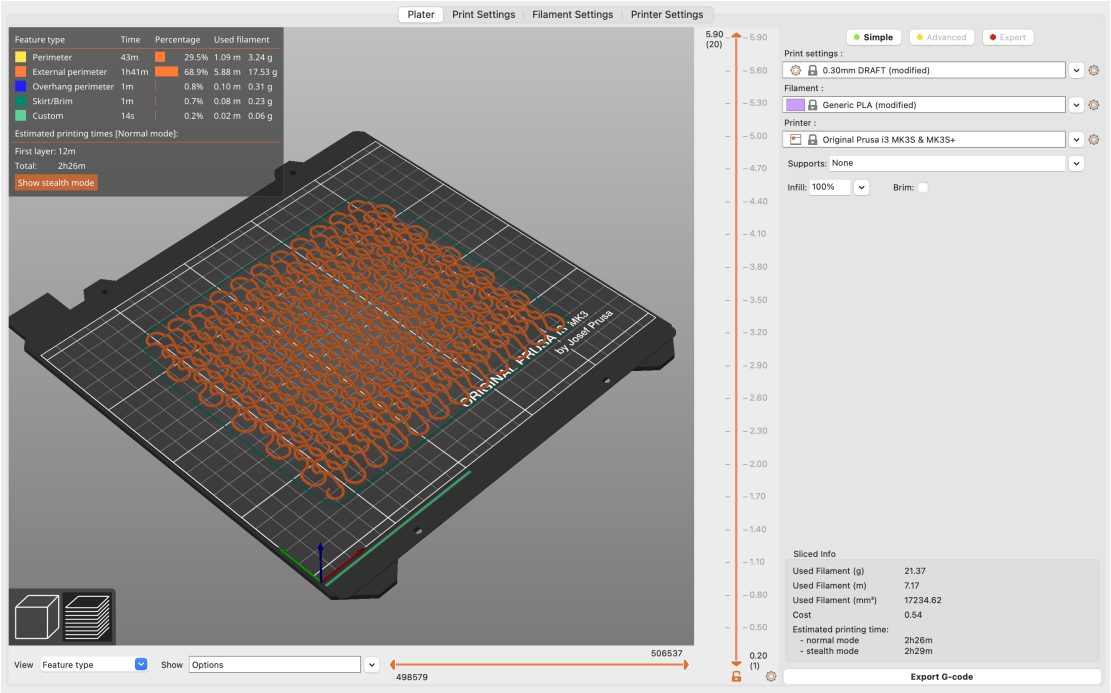

Figure 2.6: Prusa's slicing software with the base sample, with the print details

the diameter to 1.33 mm, while the *Thick Yarn* specimen increased the diameter to 2.00 mm. The number of repetitions of the base stitch was also altered. In the original version, there were 11 units in each direction. For the *Narrow* version, there were 11 units in the wale direction but only 5 in the course direction. For the *Short* version there were 5 units in the wale direction and 11 units in the course direction.

Table 2.2: The specimens printed

Specimen	Alterations from Base	Number Printed
Base	None	6
Thin Yarn	d = 1.33 mm	1
Thick Yarn	d = 2.00 mm	1
Short	course repetitions decreased	2
Narrow	wale repetitions decreased	2

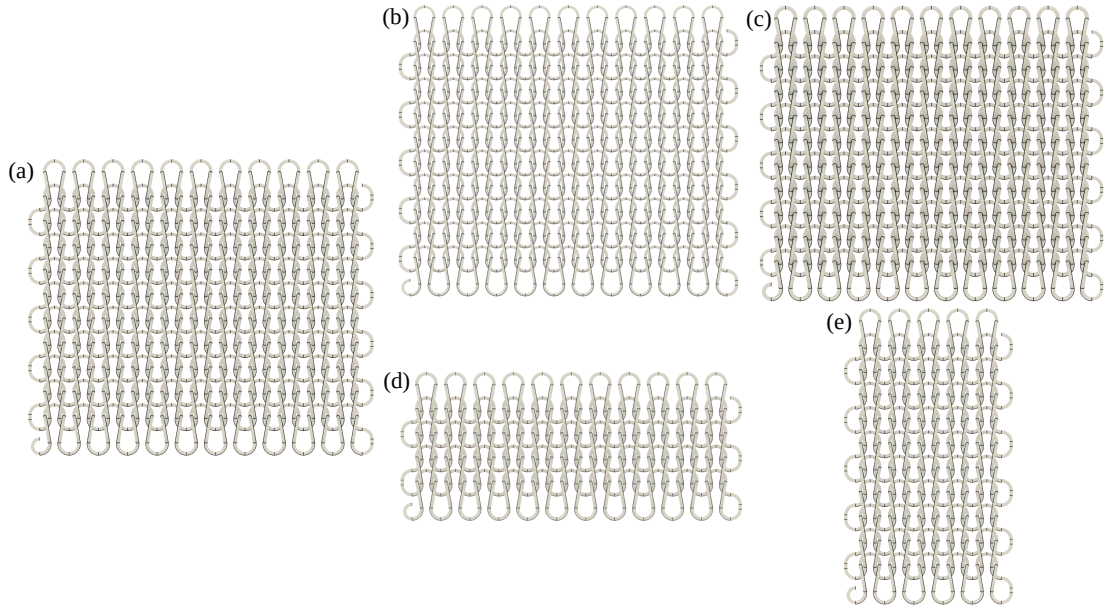

Figure 2.7: The (a) base specimen, (b) thin specimen, (c) thick specimen, (d) short specimen, and (e) narrow specimen

2.4.1 Failures and Defects

Though the majority of the prints were successful, it is worth noting that due to the complex geometry, the prints had to be supervised for the first hour of each print to ensure failures did not occur. The most common failure occurred during the first few layers, as the they were so narrow that they easily peeled off the printbed (see Fig. 2.8). Once a piece of the print came off the printbed, it would get stuck on the nozzle and cause issues for the rest of the print.

In addition to the failures, several prints finished with small defects (see Fig. 2.9). Though generally 3D printers are able to create structures with some overhang, as long as it it less than 45°, the risk of a print failure does increase a good deal. These defects were likely due to an error that occurred while printing the portion of the unit stitch that transferred from the flat arcs to the rising splines, as the printer had to deposit filament across the sections that did not have any support underneath them.

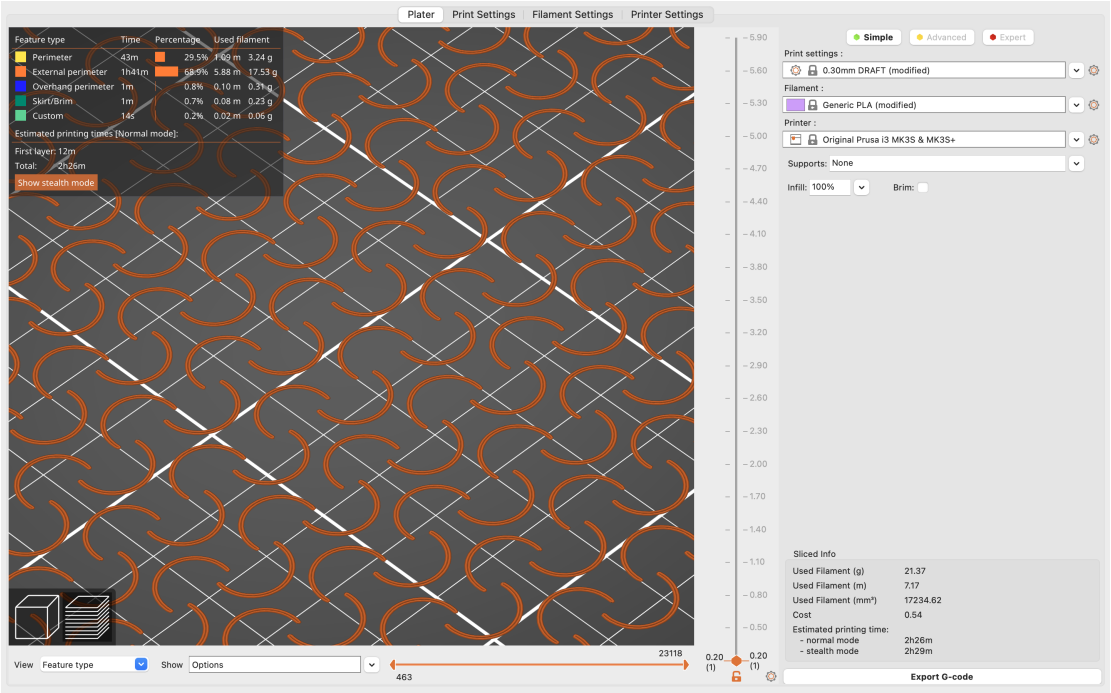

Figure 2.8: The first layer of the base specimen

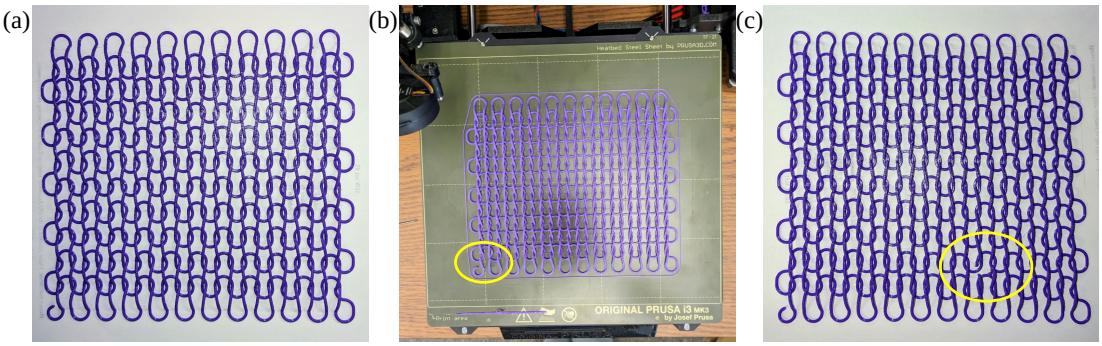

Figure 2.9: Printed base specimens without any defects (a) and with defects (b,c)

2.5 Summary

This chapter discussed the design and fabrication techniques used for the specimens. The geometry of the stitch unit was influenced by several other authors' work, as well as a sample of large-scale knit fabric. To ensure a consistency across several different drawings and assemblies, a set of parameters was developed. This geometry was used in Fusion 360 to create a 3D model, which could be replicated in the course and wale

directions in an assembly to create the final specimen. The specimen was then fabricated on a Prusa 3D printer. The next chapter discusses the experimental testing protocol used to test these specimen.

Chapter 3

Experimental Setup and Testing Protocol

3.1 Overview

Chapter 2 described how the model was created for the knit specimen. This chapter discusses the process of testing, detailing the profile of the tensile extension and cyclical testing, the procedure of setting up and conducting each test, and which specimens were tested.

3.2 Tensile Extension Testing

3.2.1 Methods

An Instron Low Force Universal Testing System (5543, Instron, Norwood, MA) was used to characterize the specimens. The main test performed was a cyclic tensile displacement-control test, where an increasing amount of extension was applied in a cyclic pattern. Fig. 3.1 shows the displacement each cycle underwent. The displacement's amplitude increased from 1 mm to 200 mm, and two cycles were performed at each amplitude. The minimum displacement was set to -1 mm to ensure the specimen had no load in between each cycle. The cycles were run at a rate of 30 mm per minute. Once the sample broke, the test was stopped.

To connect the samples to the Instron, it was important that the specimens could

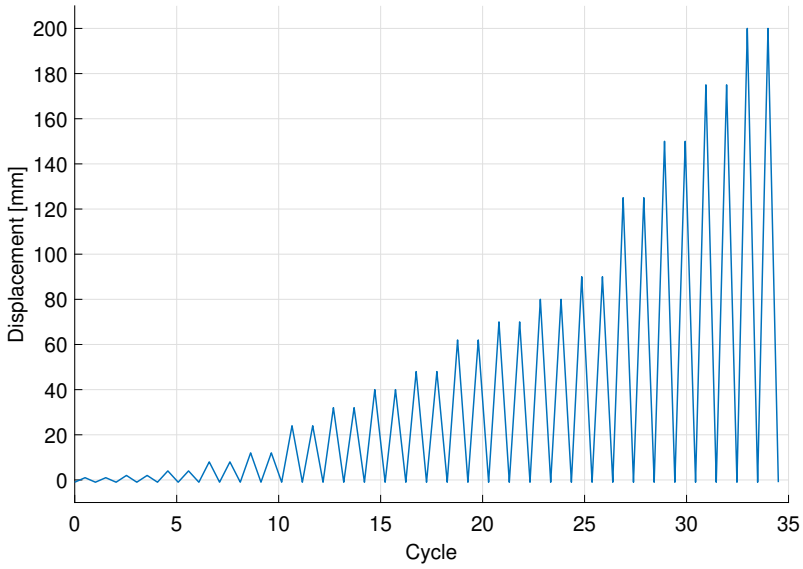

Figure 3.1: The displacement each cycle of the Instron testing underwent

rest at their full, natural extension, but also be allowed to retract when necessary. To do this, a rig was created in Fusion 360 (see Fig. 3.2). This rig had two 8-mm-diameter steel rods that were connected to the Instron machine horizontally. Hangers that could easily move across the rod were threaded onto the rods. To connect the specimens, these hangers were hooked into the edge loops of the top and bottom of the specimen. The rig was 3D printed with 30% infill. To ensure structural rigidity, the hooks were printed at 100% infill.

The majority of the tests were conducted so that the specimen's edges could contract and expand naturally in the transverse direction. However, there were several tests conducted with contraction-free edge conditions. To facilitate this, small spacers were printed and added in between the hangers to make sure the specimen would not contract as tension was applied. For testing in the course direction, spacers were set to be approximately 21 mm wide. In the wale direction they were approximately 11 mm wide. Fig. 3.3 shows the model of the course direction spacers, as well as the spacers threaded onto rod.

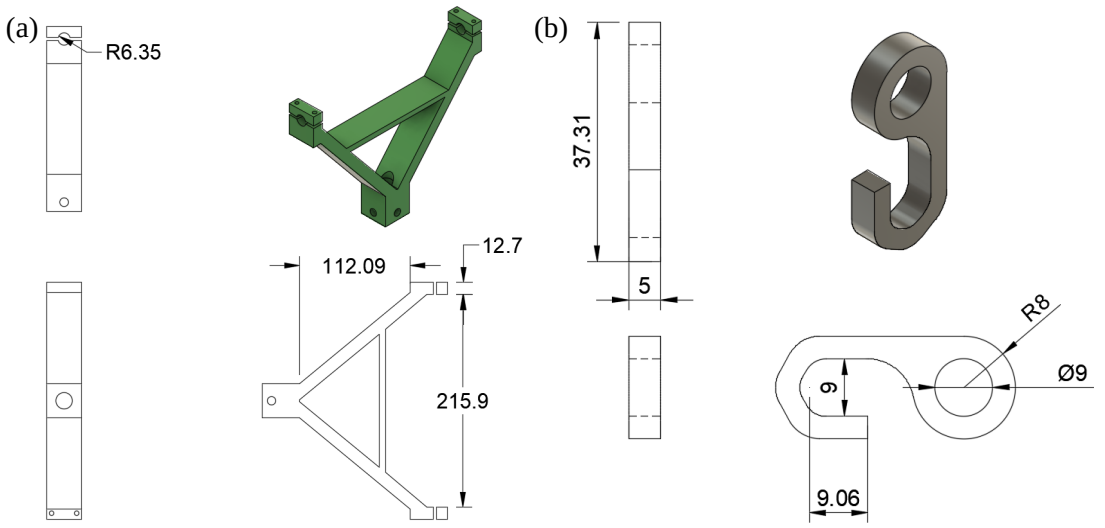

Figure 3.2: The models of the 3D printed (a) rig to the Instron machine and (b) hangers used to hook the specimens on. All dimensions shown are in mm

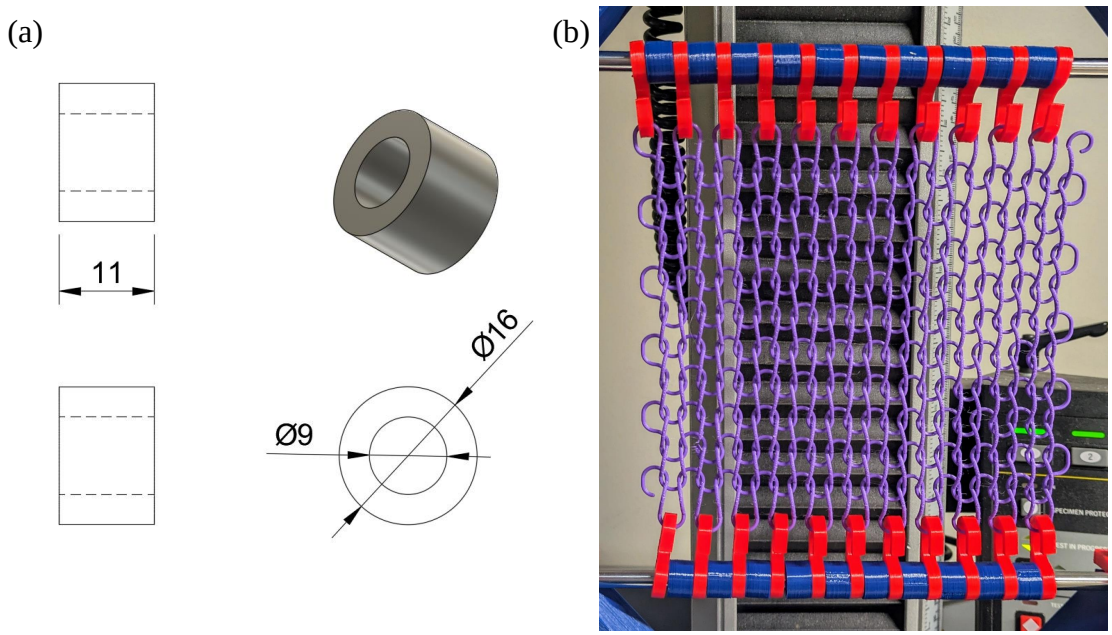

Figure 3.3: (a) The model of the 3D printed spacers, and (b) the spacers threaded onto the rod. All dimensions shown are in mm

3.2.2 Testing Protocol

After the specimens were printed, it was important to ensure they were tested in a timely manner. The time that the specimens were allowed to rest ranged from several hours

to 34 days. They were kept flat indoors to ensure there was no creep nor a a great temperature shock. They were also transported flat.

When setting up the specimens, they were first attached to the top hangers. The Instron was balanced (zeroed out), and then the specimen was connected to the bottom hangers. To calibrate the length, the Instron was brought up such that the specimen was secure, but did not have any tension. Fig. 3.4 displays the set-up of several different tests. Fig. 3.4(a) shows a test of a "Short" specimen with 6 repetitions of the unit in the course direction. Fig. 3.4(b) displays the test of a base specimen connected such that the extension is applied in the course direction, and Fig. 3.4(c) shows the same specimen such the extension is applied in the course direction.

3.2.3 Tests Conducted

While conducting tests, several factors were considered. The main concern was orientation of the test specimen (whether the course or wale direction was being stressed), and as such several tests were performed both ways on the base geometry (details in Chapter 2). Tests with spacers, in both directions, were also conducted, so that the specimen was not allowed to constrict with additional tension. The size of the "yarn" thickness, d, was also studied, as was the number of units in the course and wale directions. The last several tests performed were on specimens with the defects mentioned in Chapter 2, so that they were not put to waste. Table 3.1 goes over the parameters of each test performed.

3.3 Cyclic Testing

3.3.1 Methods

In addition to the tensile extension tests, cyclic tests were also performed to characterize the system. These tests were intended to extended the specimen up to approximately

Table 3.1: The tests performed

Specimen	Geometry	Test Direction	Spacers	Print Date	Test Date	Days Rested	Print Defect
BC1	Base	Course	No	2023/11/25	2023/12/14	19	No
BC2	Base	Course	No	2023/12/13	2023/12/15	2	No
BW1	Base	Wale	No	2023/12/14	2024/12/15	1	No
BW2	Base	Wale	No	2024/01/02	2024/01/18	16	No
BC3	Base	Course	Yes	2024/01/02	2024/02/05	34	No
BW3	Base	Wale	Yes	2024/01/10	2024/02/05	26	No
TC1	Thick	Course	No	2024/01/23	2024/02/05	13	No
NC1	Narrow	Course	No	2024/02/05	2024/02/05	0	No
NC2	Narrow	Course	No	2024/02/06	2024/02/13	7	No
SC1	Short	Course	No	2024/02/11	2024/02/13	2	No
BC4	Base	Course	No	2023/12/12	2024/12/14	2	Yes
BW4	Base	Wale	No	2024/01/09	2024/02/05	27	Yes
SC2	Short	Course	No	2024/02/06	2024/02/13	7	Yes
BC5	Base	Course[†]	No	2024/02/16	2024/03/04	16	Yes
BW5	Base	Wale[†]	No	2024/02/19	2024/03/06	16	Yes

[†]Tested in a cyclic loading pattern

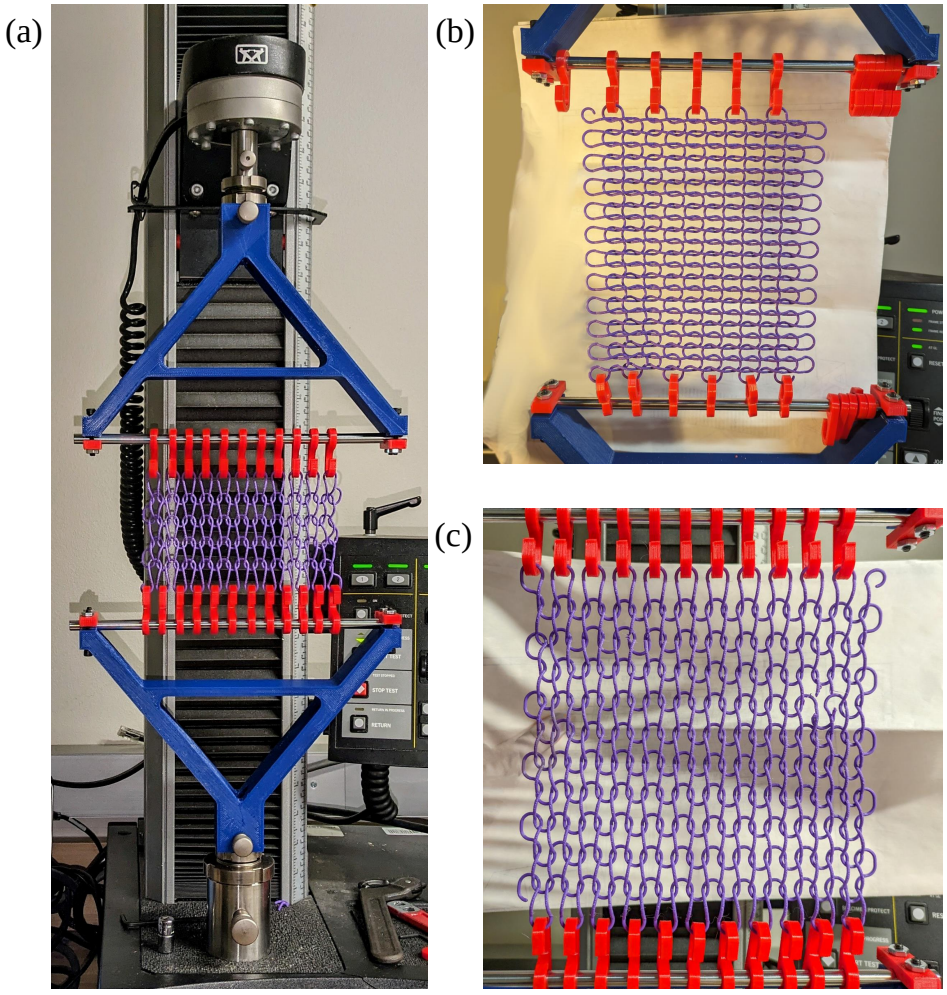

Figure 3.4: The set-up of (a) Specimen SC1, (b) Specimen BW1, and (c) Specimen BC1

90% of its maximum extension, based off the tension tests performed, release it to 70% of its maximum extension, then cycle between the two. As the amount of filament used for the previous specimens was running low, defected specimens (Section 2.4.1) were used for these tests.

3.3.2 Testing Protocol

The protocol for these tests were the same as the tensile tests.

3.3.3 Tests Conducted

Two base specimens with print defects were chosen for these tests as detailed in Table 3.1.

3.4 Summary

This chapter discussed the testing set-up and procedures for the knitted specimens. To connect the samples to the Instron machine, a rig and hangers were designed and 3D printed. Then, thirteen tests were conducted using tensile extension tests, and another two tests were conducted using cyclic loading. The majority of the tests focused testing on the base specimen developed in Chapter 2 in the wale and course direction, though tests were also conducted on specimens with altered "yarn" thickness (d) decreases in the repetition of units, as well as specimens printed with defects.

Chapter 4

Results and Discussion

4.1 Overview

Chapters 2 and 3 described how the specimens were modeled, fabricated, and tested. This chapter discusses the results found from these tests, and how the specimens were characterized.

4.2 Base Specimen

To characterize the knitted specimen, several tests were conducted with the base samples. Load-extension graphs were created to compare the tests. Active extension is shown in solid lines, while unloading is shown in a dashed line. In addition, the cycles have been color coded in a consistent manner across all tests. Tests with course extension will be in shades of blue and green, while tests with loaded in the wale direction will be in shades of red and orange.

4.2.1 Baseline Testing

First, tests were conducted in the course and wale direction without spacers to determine how the orientation of the specimen affected the specimen's behavior. In the following sections, the tests performed in these course and wale directions will be discussed, followed by a comparison of the results.

Testing in the Course Direction

Fig. 4.1 displays the load-extension curve for two base samples tested in the course direction. Consistent results can be seen for the two specimens. The samples failed at an extension of 45 mm and a load between 280 and 295 N. Specimen BC1 failed at 280.6 N, while Specimen BC2 failed at 294.9 N. Fig. 4.2 shows a close-up of the load with small amounts of extension. The darker blue lines are initial cycles, with the lighter green lines being later cycles with larger displacements. It is clear that initially applying tension in the course direction results in a higher, nonlinear stiffness than unloading the tension. As seen in Fig. 4.3, at the start of each cycle and at lower levels of extension, there is very low stiffness, close to zero. However, as the cycles increase (applying tension in the course direction) the specimens exhibit a linear, positive stiffness. During the unloading, where that tension is released, the specimen exhibits a gentle slope down, decreasing non-linearly.

There are several spots along the loading branch where the load suddenly drops, but the specimen does not fully fail. These "jumps" have two likely causes. The first is simply the specimen contracting suddenly in the direction opposite to the test direction. Though the hangers could easily move, there was some friction in the system that kept it from steadily and smoothly contracting as extension was applied. The second cause is a failure in a single unit.

The system rarely broke cleanly, as shown in Fig. 4.4. There often was one large break that caused the ultimate failure, as seen in the center of the specimen, but there were often also smaller unit failures during testing, as seen to the left of the large break. These seemed to help redistribute the force, and allowed the specimen to withstand more load. Additionally, at higher levels of tension the specimen was seen to curl in, as traditionally manufactured knitting does.

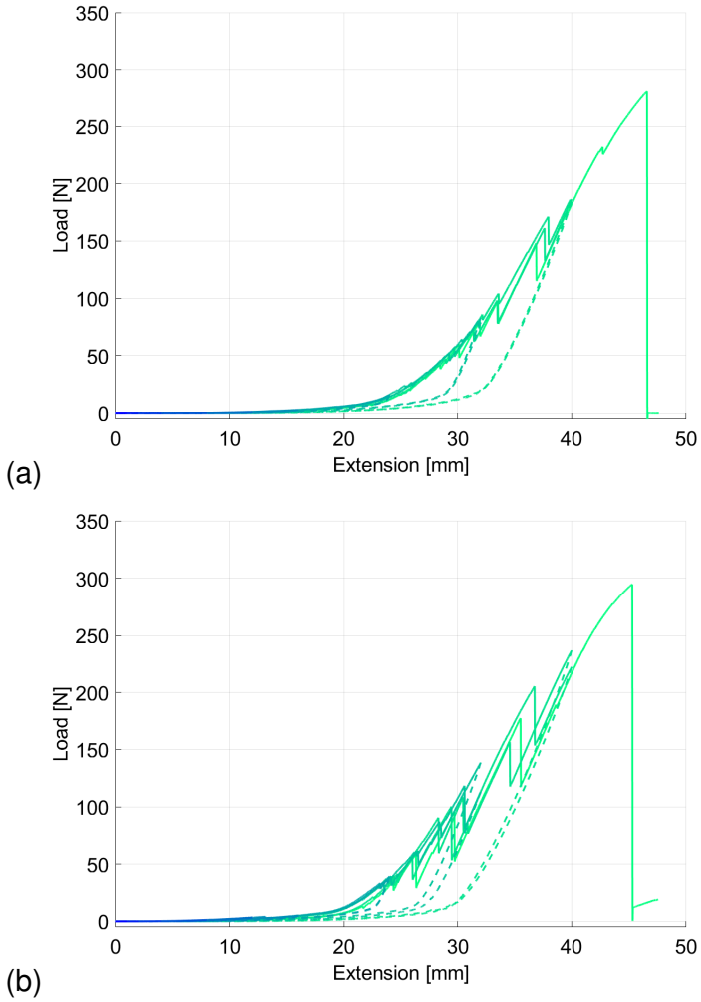

Figure 4.1: The load-extension curves for base specimen loaded in the course direction: (a) Specimen BC1 and (b) Specimen BC2

Testing in the Wale Direction

Fig. 4.5 displays the load-extension curve for two base specimens under tension in the wale direction. Samples tested under this configuration were able to withstand more extension and measured an overall lower load, typically failing at an extension of approximately 90 mm and a load between 100 and 117 N. Specimen BW1 failed at 103.3 N, while Specimen BW2 failed at 116.7 N. Fig. 4.6 shows that the loading and unloading paths differ, which results in a petal-like shape. Fig. 4.7 shows the energy for each cycle. Since each extension level has two cycles, each level has two dots. The larger

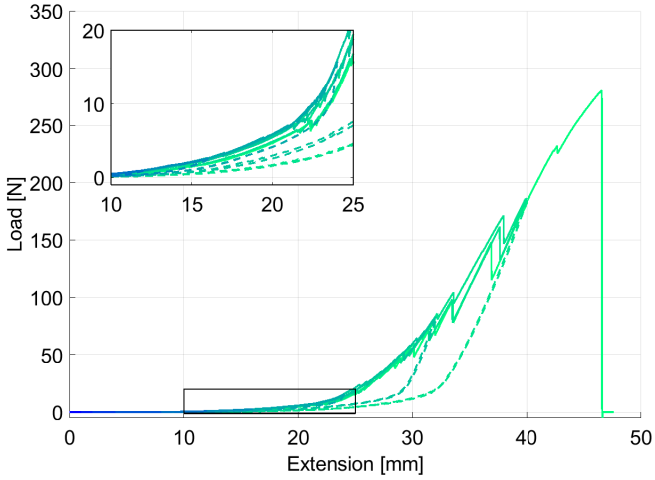

Figure 4.2: The load-extension curves for Specimen BC1, with a close-up of the initial loading

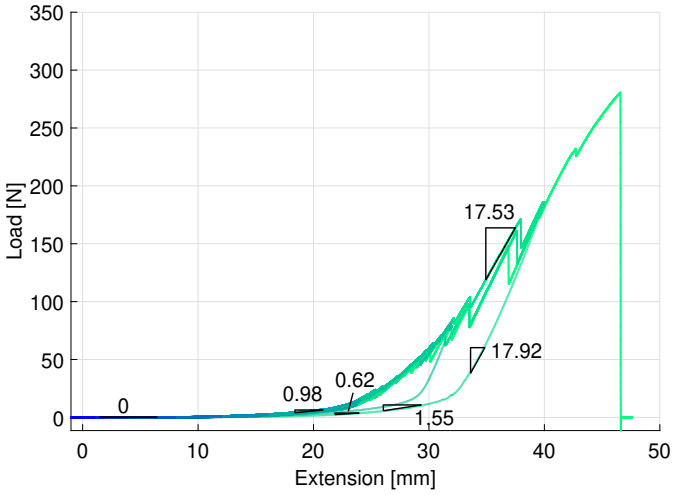

Figure 4.3: The load-extension curves for Specimen BC1, with stiffness noted

amount of energy is always the first dot, as the specimen undergoes a permanent deformation at each extension level. There is still some residual strain in the system though, as the energy does not drop to zero, it just has less resistance and therefore a lower amount of energy. The specimen also does not recover fully, as there is always energy at the next extension level. In addition to the permanent deformation at each extension level, as the extension increases, as does the energy. This means the unique petal shape is likely due either yielding, creep, or relaxation. This petal shape is very distinctive from the linear, positive stiffness in course testing, allowing the loading pattern to eas-

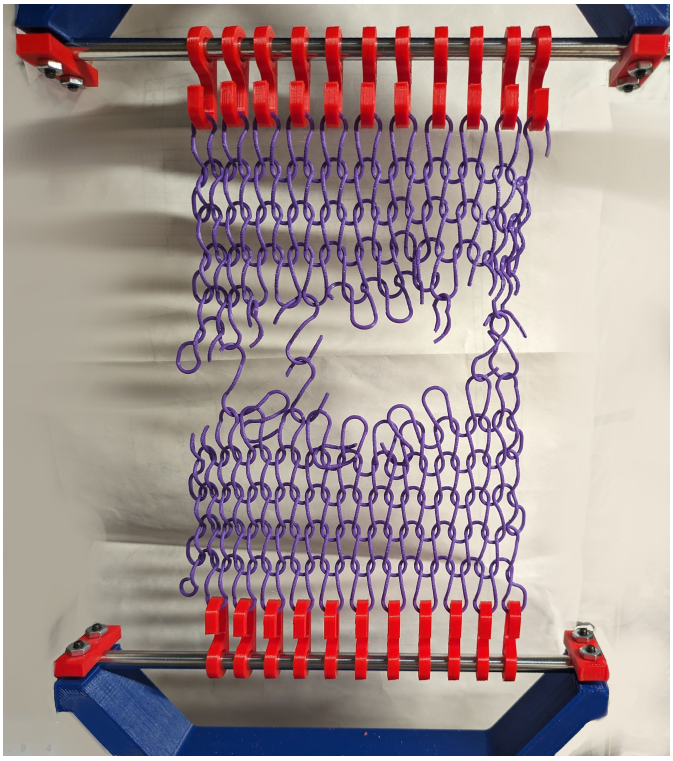

Figure 4.4: The broken Specimen BC2 after undergoing tensile extension in the course direction

ily be discerned from the load-extension graph. Additionally, "jumps" in load are not observed as often in specimens loaded in the wale direction as they were in specimens loaded in the course direction.

Comparison of Course and Wale Testing

Fig. 4.8 displays the load-extension curves for two base specimens under course and wale extension. It is obvious that the specimens have some anisotropy, as they have quantitatively and qualitatively different responses.

Visual inspection of the specimen under tensile extension showed that when extension was applied in the course direction, the units appeared to "lock" out quite early, while when tension was applied in the wale direction the specimen had more give and was able to flex. This is corroborated by Fig. 4.8 which show a drastic difference between the amount of extension the specimens under tension in the wale direction and

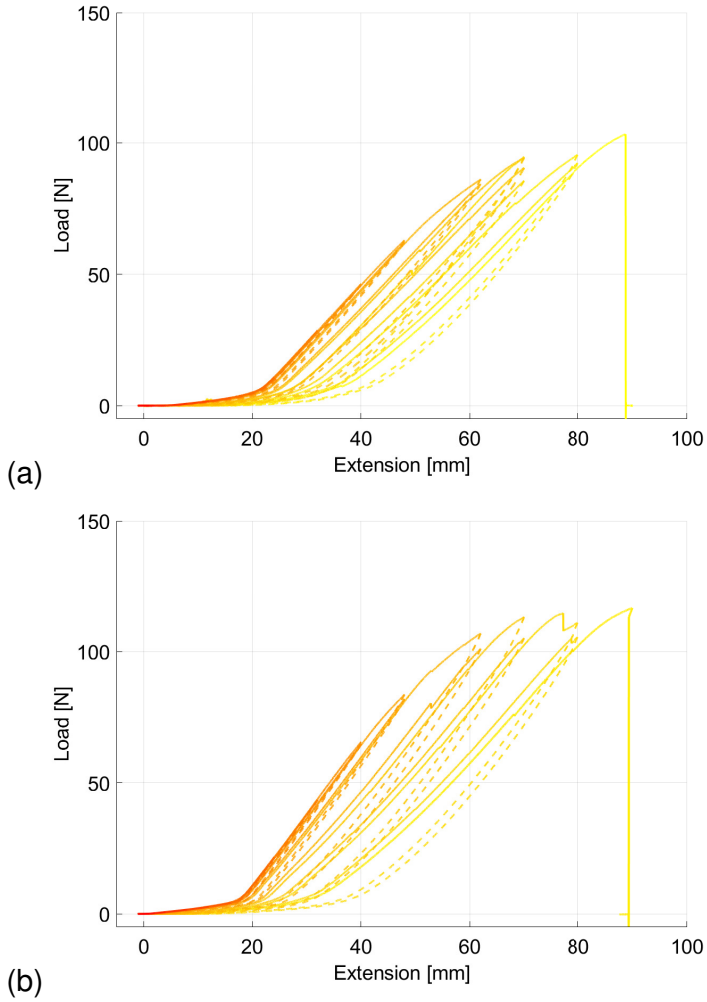

Figure 4.5: The load-extension curves for base specimen loaded in the wale direction: (a) Specimen BW1 and (b) Specimen BW2

specimens under tension in the course direction are able to withstand.

Effect of Rest Time

The base system was tested twice in each direction, and each specimen had different resting times from printing to testing. Figs. 4.1 and 4.5 each had a newer specimen, allowed to rest less than a week, and an older specimen, allowed rested over two weeks. In Fig. 4.1 the specimen is tested with extension in the course direction, (a) is the older specimen and (b) is the newer. The older specimen appears to have fewer "jumps" than the newer specimen. The newer specimen's failure load is 5% higher than the older.

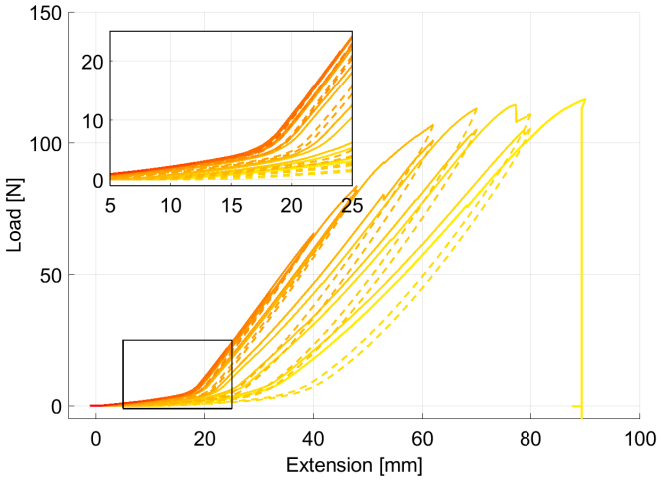

Figure 4.6: The load-extension curves for Specimen BW2, with a close-up of the initial loading

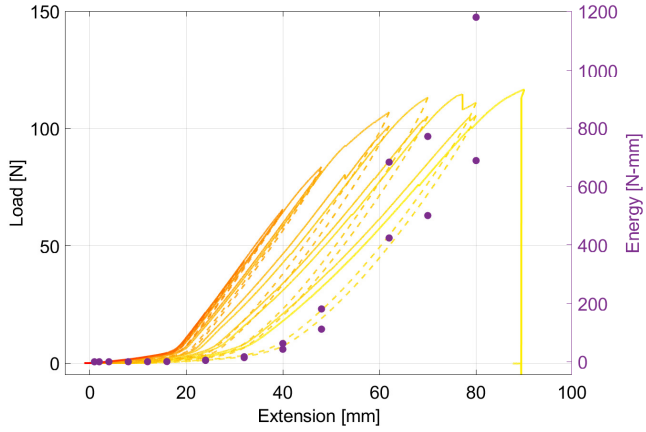

Figure 4.7: The load-extension curves for Specimen BW2, with energy at each cycle plotted as dots on the right axis

The extension at failure is less than 3% lower than the older specimen's extension at failure. In Fig. 4.5 the specimen is tested with extension in the wale direction, (a) is the newer specimen, (b) is the older. The newer specimen has a load that is nearly 13% higher than the older specimen and the extension is 1% lower than the older specimen's extension at failure. Therefore, it can be concluded that while the newer specimens may resist a higher load, the final extension failure point does not significantly change. Ultimately, the time that a specimen is allowed to rest between print and test does not appear to result in significant changes.

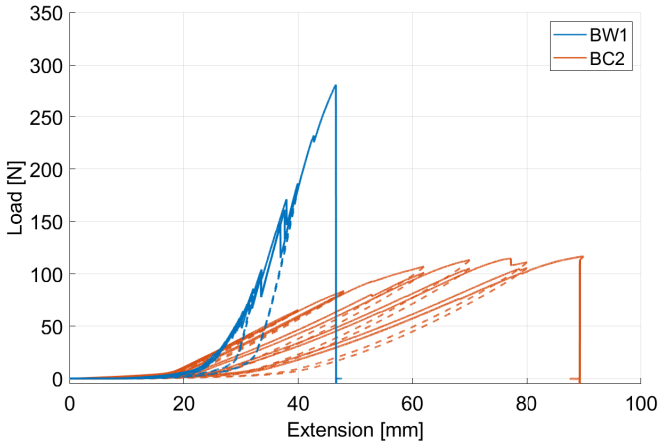

Figure 4.8: The load-extension curves for two base specimen loaded in the course (Specimen BC1) and wale (Specimen BW2) directions

4.2.2 Tests Performed with Spacers

After tests of the base specimen were conducted in both the wale and the wale direction, tests were ran with spacers to see the effect of prohibiting contraction in the direction opposite of the extension.

Tests in Course Direction

Fig. 4.9 shows the load-extension curve for Specimen BC3 loaded in the course direction, with the failure point at an extension of 34 mm and a loading of 189.1 N. This is slightly less extension than the base specimen (Fig. 4.1), but the base specimen had 56% greater ultimate load. The stiffness while the specimen is being loaded is approximately 15 to 22 N/mm, which is not significantly different to the stiffness of the original system.

It is interesting to note that at the extension of 32 mm there was a higher loading, approximately 190 N. Based off the failure seen in Fig. 4.10 and the fact that the specimen was not allowed to contract, the drop between 32 and 34 mm is likely due to one of the “jumps” due to unit failure as mentioned in Section 4.2.1.

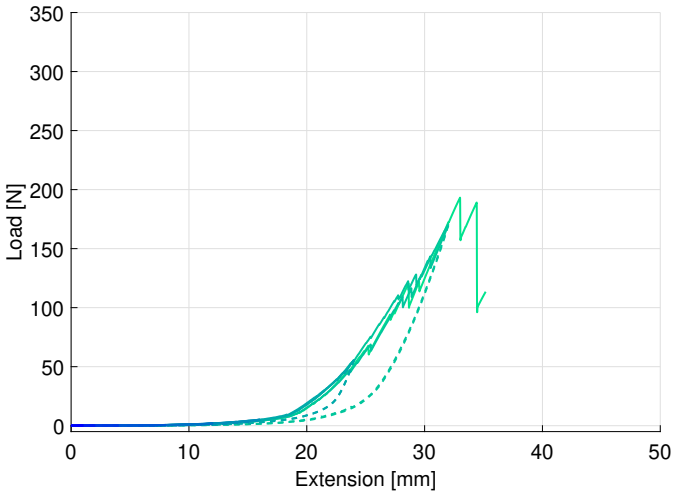

Figure 4.9: The load-extension curve for a base specimen with spacers (Specimen BC3) loaded in the course direction

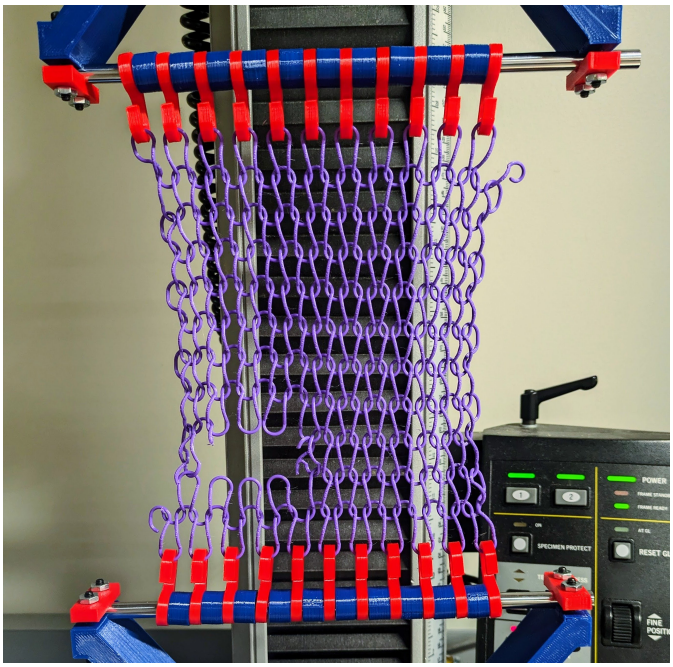

Figure 4.10: The base specimen with spacers (Specimen BC3) after undergoing tensile extension in the course direction

Testing in the Wale Direction

Fig. 4.11 shows the load-extension graph of Specimen BW3 loaded in the wale direction, with the maximum extension of 80 mm and with a loading of 116 N. Similar to Specimen BC3, this specimen had a similar level of extension to the base specimen

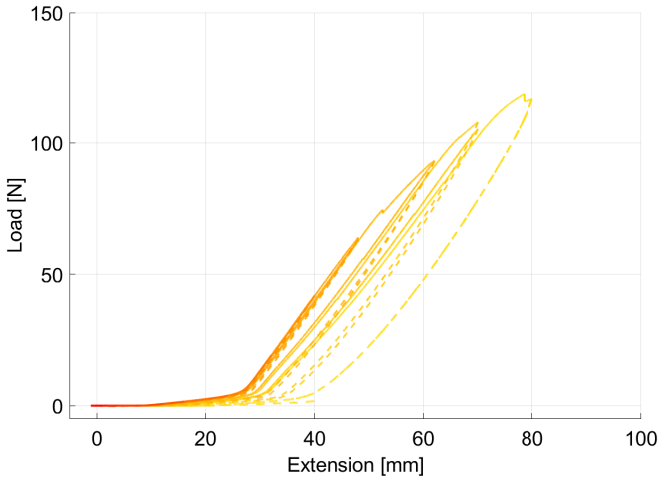

Figure 4.11: The load-extension curve for a base specimen with spacers (Specimen BW3) loaded in the wale direction

(Fig. 4.5), but a slightly lower level of force. In this case, the maximum load of the specimen tested with spacers was 12% lower than the maximum load of the specimen tested without. Unlike the graphs previously shown, this did not have a sharp drop-off to indicate failure. This is likely because, unlike all previous tests, this specimen did not break in the middle, but instead at the edge loops. Fig. 4.12 shows the failed sample. Though the majority of the sample is in once piece, the test would have had to be restarted to see a more traditional failure, so it was stopped there.

4.3 Non-Base Specimen

4.3.1 Thick and Thin Specimens

Though both "thick" and "thin" specimens were modeled, only the thick sample was able to be successfully printed, and thus it was the only one that was able to be tested. Fig. 4.13 shows the load-extension graph for the thick specimen (Specimen TC1) tested in the course direction, showing that this sample failed at a 40 mm extension and 465 N load. This is 12% less extension than the base samples (Fig. 4.1) were able to undergo, but the specimen's load was able to withstand a load 58% higher than the base

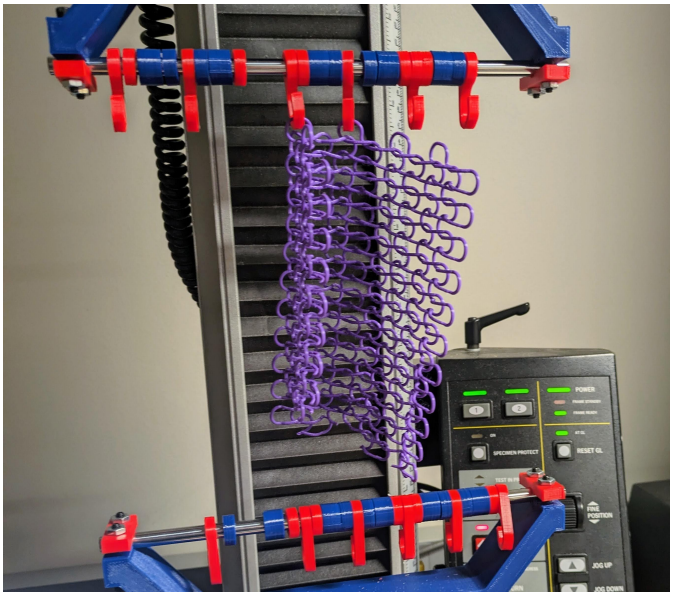

Figure 4.12: The broken base specimen with spacers (Specimen BW3) after undergoing tensile extension in the wale direction

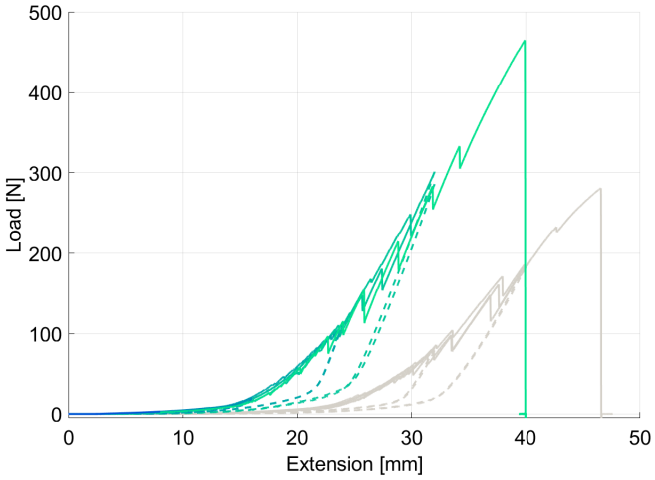

Figure 4.13: The load-extension curve for the thick specimen (Specimen TC1) loaded in the course direction. Specimen BC1's load-extension curve is shown in grey

specimen's load. The stiffness was also slightly higher, ranging from 15 to 30 N/mm.

4.3.2 Narrow Specimen

Two "narrow" specimens were tested. These had with half the number of course units as the base specimens. Fig. 4.14 shows the narrow specimens tested with extension in the

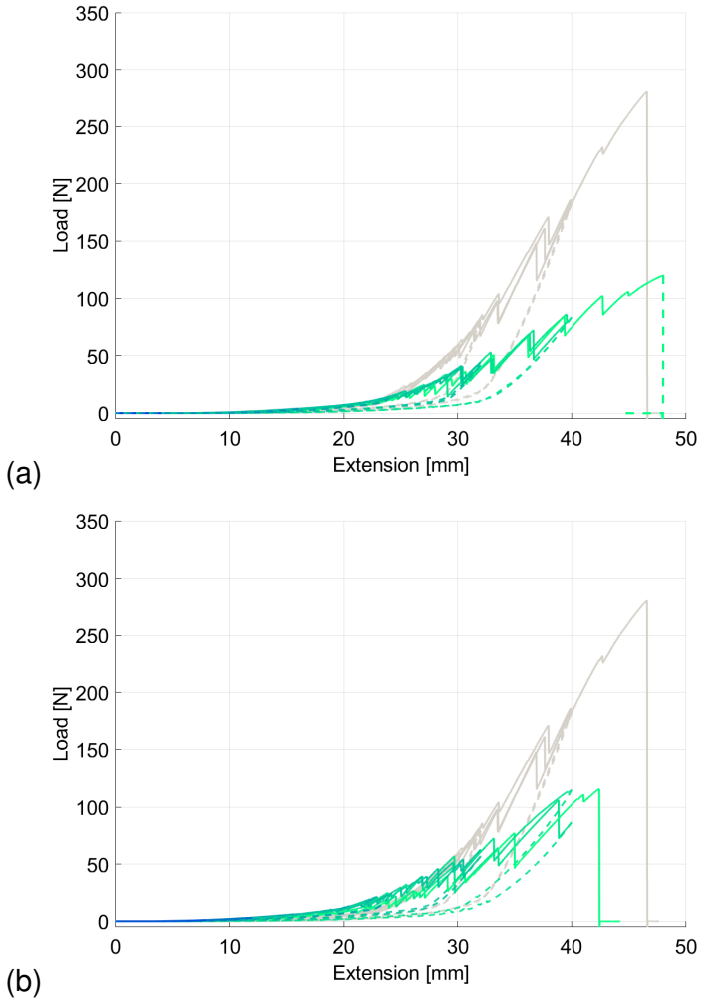

Figure 4.14: The load-extension curve for narrow specimen loaded in the course direction: (a) Specimen NC1 and (b) Specimen NC2. Specimen BC1's load-extension curve is shown in grey

loading direction. Specimen NC1 failed with a 48 mm extension and 120 N load, while Specimen NC2 failed at a 45 mm extension and a 115 N load. While these samples had 60% lower ultimate load than the base specimens (Fig. 4.1), the extension is almost identical. Additionally, these specimens do not have the same unit failures or "jumps" as the short or the base specimen specimen did.

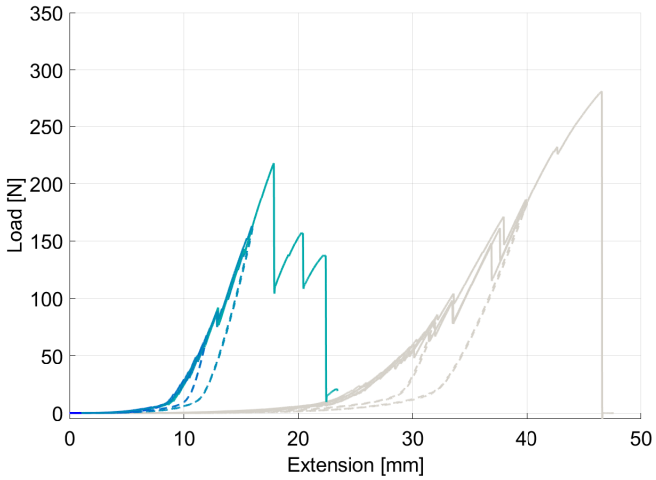

Figure 4.15: The load-extension curve for a short specimen (Specimen SC1) loaded in the course direction. Specimen BC1's load-extension curve is shown in grey

4.3.3 Short Specimens

One "short" specimen (Specimen SC1) was tested. It had with half the number of wale units as the base specimens. Fig. 4.15 shows that Specimen SC1 failed at a 22 mm extension and 138 N load. This is 51% less extension and 53% less load that the base specimen (Fig. 4.1) was able to withstand. Interestingly, the system sees several "jumps" right before the final failure point, which means the failure point was not the maximum load that the sample was able to withstand. The absolute maximum load was at 18 mm, with a load of 217 N, which has a load of only 26% less than the base specimen. Fig. 4.16 shows the failed specimen and it is clear that there are several failure spots, which means these jumps were caused by smaller, unit failures across the specimen.

4.4 Specimens with Print Defects

The specimens with print defects mention in Section 2.4.1 were also tested.

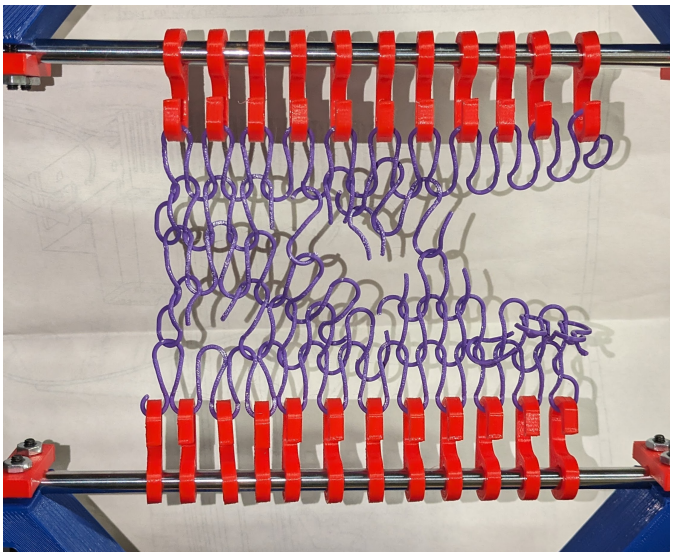

Figure 4.16: Specimen SC1 after undergoing tensile extension in the course direction

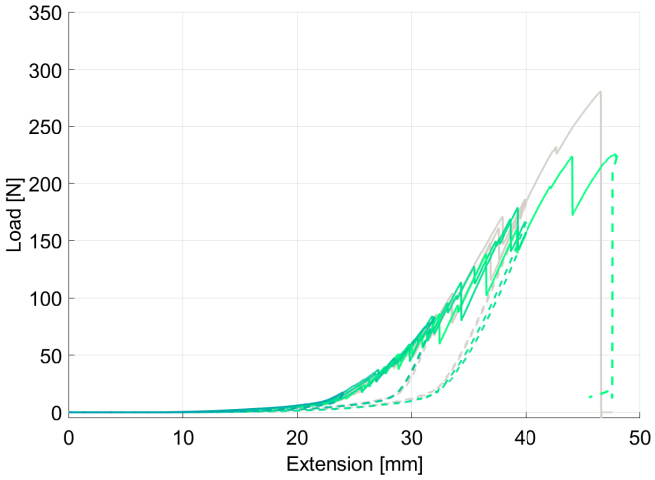

Figure 4.17: The load-extension curve for defective Specimen BC4 loaded in the course direction. Specimen BC1's load-extension curve is shown in grey

4.4.1 Testing in the Course Direction

Fig. 4.17 shows a base specimen with defects tested in the course direction, failing at a 48 mm extension and 224 N load. This is very similar to the base specimen without defects (Fig. 4.1), though it does allow for around 6% more extension and around 24% less load.

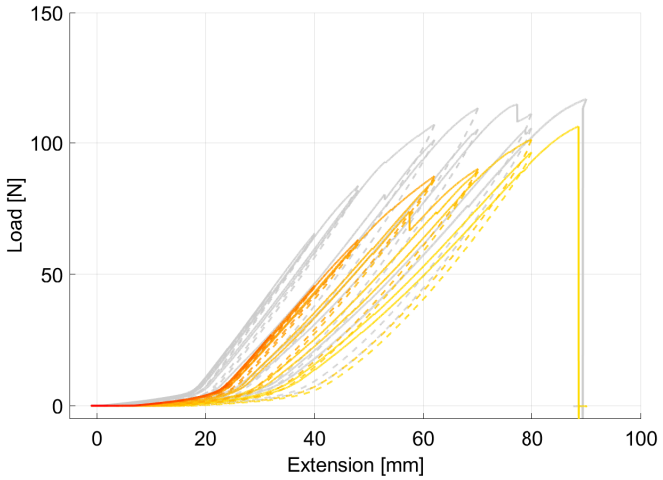

Figure 4.18: The load-extension curve for defective Specimen BW4 loaded in the wale direction. Specimen BW2's load-extension curve is shown in grey

4.4.2 Testing in the Wale Direction

Fig. 4.18 shows a base specimen with defects tested in the wale direction, failing at a 88 mm extension and 106 N load. This is very similar to the base specimen without defects (Fig. 4.1), though it could withstand around 2% less extension and slightly less load.

4.4.3 Testing with a Short Specimen

Fig. 4.19 shows a short specimen with defects tested in the course direction, failing at a 23 mm extension and 240 N load. Though the extension is similar, the load is nearly twice the non-defected load. This performance may be due to the defects acting as built-in failure points. As the weak, defected regions fail, that allows the stress to redistribute around the rest of the structure. The reason this was not seen as prominently in the base specimens is as they have a larger area originally, so the stress redistribution has less of a drastic effect.

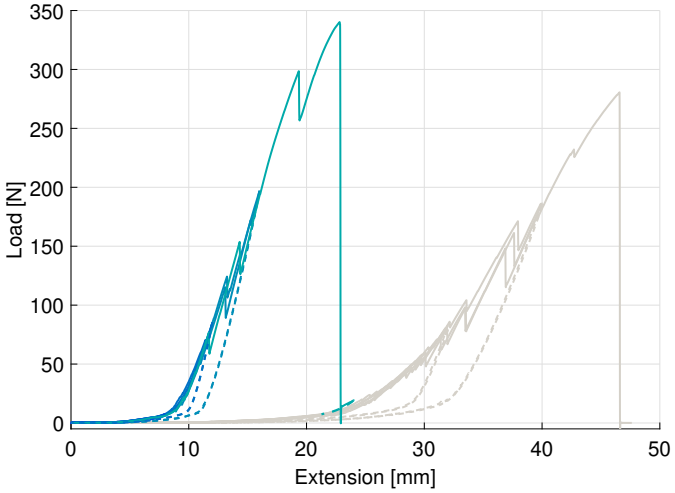

Figure 4.19: The load-extension curve for defective Specimen SC2 loaded in the course direction. Specimen BC1's load-extension curve is shown in grey

4.5 Cyclic Tests

4.5.1 Testing in the Course Direction

For the cyclic test in the course direction, the specimen was cycled between 30 mm and 40 mm. The load-displacement curve is shown in Fig. 4.20. The test ended after the Instron machine timed out, though there were several unit fractures in the specimen. The maximum load found is 261.6 N, which is comparable to the loads found with the other defected specimens that underwent extension in the course direction. As the test progresses, the load smoothly, but significantly, decreases. On the last test, the load was 50 N, nearly 80% lower than the initial maximum load. However, most of the larger drops are due to sudden jumps, similar to those seen in previous tests. Though there are several jumps on the first cycle due to the specimen contracting in, the are also several jumps during the remainder of cycles. These typically happen towards the end of the cycle, and it is shown by the load suddenly dropping. These are all due to small, unit fractures. The close-up in the upper-left hand corner of Fig. 4.20 shows several of the jumps without the intermediate cycles.

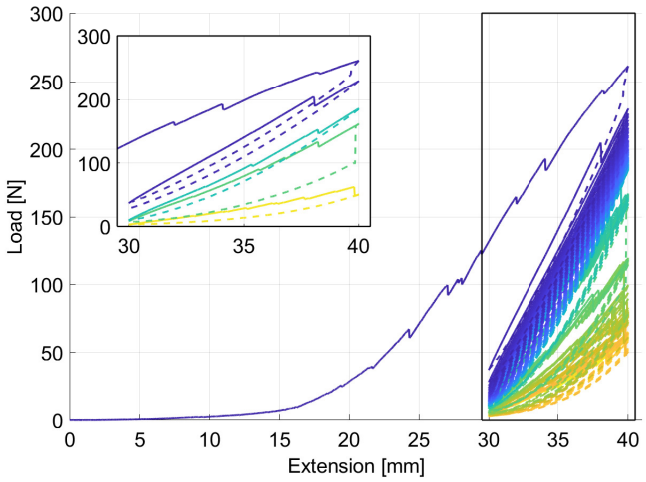

Figure 4.20: The load-extension curve for defective Specimen BC5 loaded cyclically in the course direction. A close-up is presented in the upper left-hand corner with a limited number of cycles shown

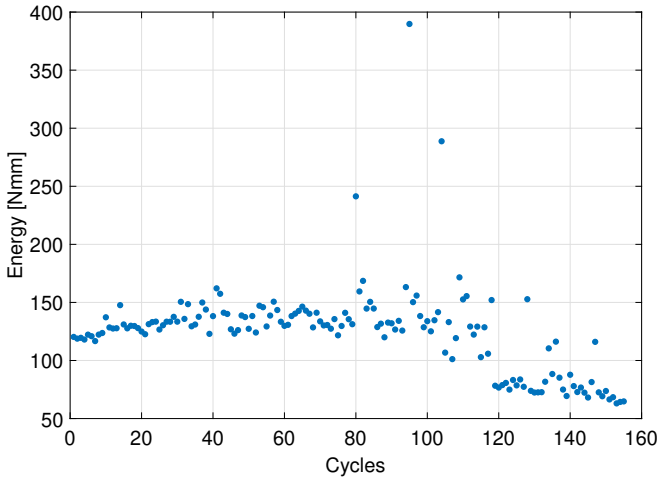

Figure 4.21: The energy for defective Specimen BC5 loaded cyclically in the course direction

The energy was also found for this system. As there is a drastic drop in load after the first cycle, there is also a large amount of energy. Spikes in the amount of energy afterward correspond to unit fractures.

4.5.2 Testing in the Wale Direction

For the test in the wale direction, the specimen was cycled between 85 mm and 75 mm. The load-displacement curve is shown in Fig. 4.22. The specimen was not able

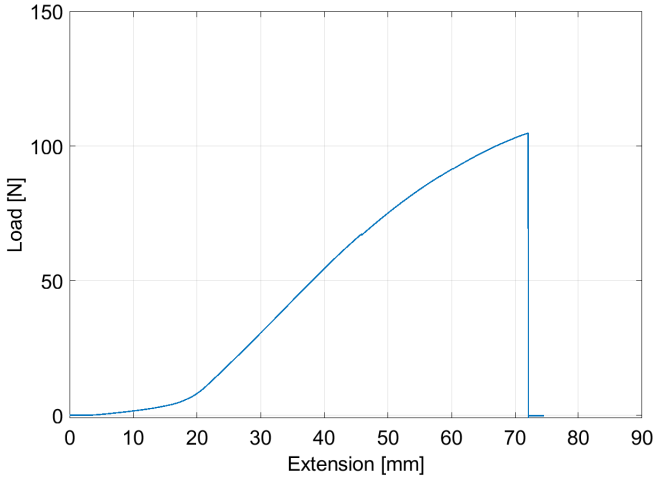

Figure 4.22: The load-extension curve for defective Specimen BW5 loaded cyclically in the wale direction

to withstand 85 mm extension. Though previously tested base specimens printed with and without defects were able to be extended to 90 mm, this specimen was only able to withstand 72 mm of extension, with a load of 104.8 N. The amount of load is comparable to the previously tested specimens. The lower maximum extension is possibly due to the fact that with the initial loading done in one cycle, the specimen was unable to stabilize. Unlike the specimen tested in the course direction, there are no jumps. The load-displacement graph very clearly displays a bi-linear stiffness at the beginning of the cycle, with a nonlinear stiffness as it reaches its maximum extension.

4.6 Normalized Comparisons

To better understand the true effect of the change in geometry, the load and extension were normalized. To normalize the load, the measured load F was divided by the nominal ultimate load F_u:

$$F_{\text{normalized}} = \frac{F}{F_u} = \frac{F}{f_u \times A} = \frac{F}{f_u \times [\pi(d/2)^2 \times N]} \tag{4.1}$$

where f_u represents the manufacturer's tensile strength (PolyMaker, 2018) and A is the

nominal cross sectional area of the specimen. This area is calculated based on the "yarn" diameter d and the number N of "yarns" on the potential failure plane. For the base, short, and narrow specimens tested in the course direction, N is taken to be 23, 23, and 12, respectively; for the base specimen tested in the wale direction, N is taken to be 11. To normalize the length, the measured extension δ was divided by the length L of the specimen:

$$\delta_{\text{normalized}} = \frac{\delta}{L} \tag{4.2}$$

For the base, short, and narrow specimens tested in the course direction, L is taken to be 152, 76, and 152 mm, respectively; for the base specimen tested in the wale direction, L is taken to be 177 mm. The normalized load-extension plots are shown in Fig. 4.23, and the normalized ultimate load and extensions can be seen in Table 4.1. When the tests in the course direction (Fig. 4.23(a)) are compared to each other, they all exhibit similar behavior, with the curves nearly collapsing on top of each other; the slight discrepancy could be due differences in the level of engagement of the specimen at the start of the test. Moreover, the normalized ultimate loads (Table 4.1) are all comparable. Likewise, the tests in the wale direction (Fig. 4.23(b)) collapse onto each other, with very similar ultimate loads. However, when comparing the course- and wale-direction tests, different behavior is observed, as previously noted, indicating anisotropic behavior. Notably, the normalized ultimate loads for the tests in the wale direction are lower than those in the course direction, which is likely due to the difference in stress distributions developed in the two loading directions.

4.7 Summary

This chapter discussed the final results of the tests conducted. The specimens were characterized by testing in tensile extension and comparing load-extension graphs, as well

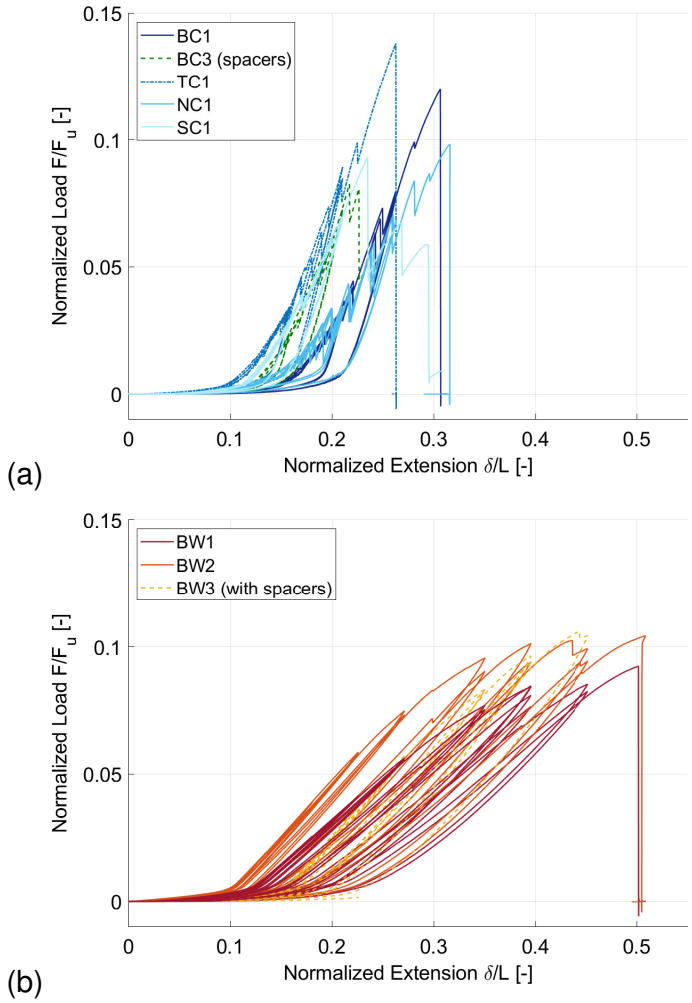

Figure 4.23: The normalized load-extension curves for tests with extension in the (a) course direction and (b) wale direction

as their ultimate failure load and extension (see Table 4.1). Specimens that were extended in the course direction showed a sharp increase in load, typically failing around 45 mm extension with a load of around 290 N. Specimens extended in the wale direction had a different loading and unloading pattern, which resulted in a petal-like shape, typically failing around 90 mm with a load of around 110 N. It was noted that the units appeared to "lock" out quite early in the course direction, while the wale direction was able to flex. The load-extension graphs often showed "jumps" where the piece appeared to begin its failure, but did not fail completely. These were likely due to sudden contrac-

tion or small, unit failures. Adding spacers appears to lower the amount of extension that the system can withstand, but the ultimate load is also lower. This is more apparent in course extension. Rest time between printing and testing did not appear to have a significant impact on the system. Thick specimens had far larger ultimate load, but could withstand about the sample amount of extension. Narrow specimens were able to extend approximately the same amount as the base specimens, with approximately one-third of the ultimate load. Short specimens were able to withstand about half of the extension, with comparable loads on average. Base specimens with defects did not appear to have significant benefits or disadvantages over specimens without defects, but

Table 4.1: The ultimate load and extension of each specimen, compared to the normalized ultimate values. The course specimens are compared in the first half, the wale in the second

	Dimensional		Normalized	
Specimen	Load (N)	Extension (mm)	Load (–)	Extension (–)
BC1	280.6	45	0.120	0.296
BC2	294.9	45	0.126	0.296
BC3$^{\|\|}$	189.1	34	0.081	0.224
TC1	464.7	40	0.138	0.263
NC1	119.8	48	0.098	0.316
NC2	115.9	45	0.095	0.296
SC1	137.4*	22	0.059*	0.289
BC4§	225.5	48	0.096	0.316
SC2§	340.2	22	0.130	0.289
BC5†	n/a	n/a	n/a	n/a
BW1	103.3	89	0.092	0.503
BW2	116.7	90	0.104	0.508
BW3‡¶	116.7	80	0.104	0.452
BW4§	105.5	89	0.094	0.503
BW5$^{\S\|\|}$	104.8	72	0.094	0.407

¶Tested with spacers

§Specimen with print defect

*Peak load measured to be 217.8 N, corresponding to a normalized load of 0.093

†Cyclic load test for which failure did not occur

‡Ultimate corresponds to maximum extension, not failure point

$^{\|\|}$Cyclic test

when a short specimen with defects sample was tested it was found to have built up a far larger force than the original sample. When tested in a cyclic pattern, the course specimen was shown to have a decreasing load and several jumps. Most of the jumps were due to unit fractures in the specimen. Energy was found to increase during these fractures. The wale specimen failed earlier than previous tests, possibly because the specimen was unable to stabilize with higher levels of stress. Finally, comparing normalized load and extension data shows that the stresses and strains of a specimen of knit PLA do not change with geometric alterations.

Chapter 5

Summary, Conclusions, and Future Work

5.1 Summary and Conclusions

Knitting is the process of making textiles with two or more needles through the process of "interlooping." The needles are used to manipulate the yarn to to draw a new loop through the existing ones. With certain patterns of knitting, the textile curls in on itself in a self-actuating process. This property can be manipulated to form many different shapes (Kamien, 2022; Amanatides et al., 2022). Current literature exploring engineering applications of knitting focuses on using yarn and knitting machines, and for structures an additional rigid element must be added (Gupta et al., 2020; Sun et al., 2023). The overall goal of this energy was to model and fabricate a specimen of knit material using additive manufacturing, specifically FDM, then characterize the specimen.

Before printing, the geometry of knitting was studied and modeled in Fusion 360 as a single unit stitch that could be replicated in the wale and course directions into a larger specimen. A set of parameters was established across the various models to maintain consistency. The specimen was fabricated on a Prusa printer, and then let rest before testing. Several different variations of the specimen were made. These included a base sample which had the same number of stitch units in the wale and course direction, specimens with altered "yarn" diameters, and specimens that had decreased the number

of course or wale repetitions. Unfortunately, due to the complex design there were several prints with defects.

To characterize the samples, they were tested in tensile extension and under cyclic loading. Load-displacement graphs were used to compare tests. A rig and hangers were designed in Fusion 360 and printed on a Prusa printer, though with a far larger infill than the specimens to maintain structural rigidity, to connect the specimen to the Instron machine. Specimens were extended in the wale and course directions, and these exhibited very different results. It was found that specimens extended in the wale direction failed around 45 mm with a load of approximately 290 N while specimens extended in the course direction failed at around 99 mm with a load of approximately 110 N. Stitch units appear to "lock" out when tension is applied in the wale direction, which limits the amount of extension that a specimen could withstand. However, in the course direction the specimen was allowed to flex. Additionally, the load-extension graphs on wale and course loading displayed "jumps," where the specimen appeared to begin its failure, but did not fail completely. These were likely due to sudden contraction or small, unit failures. The amount of time between printing and testing did not appear to have a significant impact on the system. Adding spacers in between the hangers to limit the contraction of the specimen lowered the amount of extension that the system could withstand, as well as lowering the ultimate load. This is is more apparent in wale extension. Specimens with a larger diameter d, or a thicker "yarn," had far larger ultimate load, but could withstand about the same amount of extension. Specimens that had half the number of repetitions of the unit stitch in the wale direction ("short") were able to withstand about half of the extension, with similar ultimate loads on average. Specimens that had half the number of repetitions of the unit stitch in the course direction ("narrow") were able to extend approximately the same amount as the base system, with approximately one-third of ultimate the load. Base specimens with defects did

not appear to have significant benefits or disadvantages over specimens without defects. Although, when a short specimen with defects was tested it was found to have sustained a far larger load than the original sample. When tested in a cyclic pattern, the wale specimen was shown to have a decreasing load and several jumps. Most of the jumps were due to unit fractures in the specimen. Energy was found to increase during these fractures. The course specimen failed earlier than previous tests, possibly because the specimen was unable to stabilize with higher levels of stress.

Ultimately, it was found that specimens that were put under tensile loading were able to withstand more extension when the load was in the course direction. The thickness of the "yarn" does not matter, though the ratio of the number of repetitions of the unit stitch in the course and wale direction may. Thus, the specimen was shown to have anisotropic behavior, similar to that of textile knitting. The source of this behavior is not yet fully understood, but it is likely that it is partially due to the lattice structure of the knit model as well as the anisotropy that is inherent to many additive manufactured specimens. Additionally, stresses and strains of a specimen of additive manufactured knitting do not change with geometric alterations.

5.2 Future Work

Though the basic material behavior of the specimens was qualified, not much work was done in understanding how to manipulate the curling, anisotropic behavior inherent to knitting. As seen in Fig. 5.1(a) and (b), when the specimens are pinned on one side and let hang. When the print-bed side is up, the specimen folds over at the first course row (a), while when the print-bed side is down it keeps it shape (b). This mean the specimen can easily be rolled when rolling with one side down, but if the specimen is flipped it will keep it's shape. When applying some compression on either side, the specimen forms into a dome-like shape, as shown in Fig.5.2. When compression is applied in the

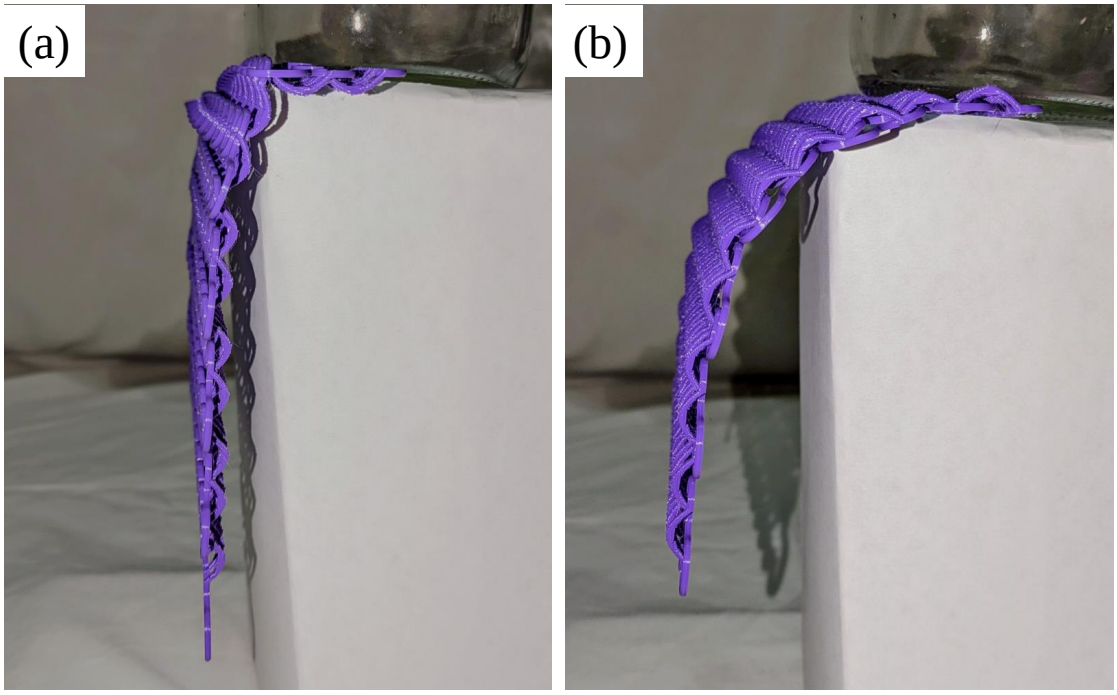

Figure 5.1: The anisotropic behavior base specimen while loosely hanging with the print-bed side (a) up and (b) down

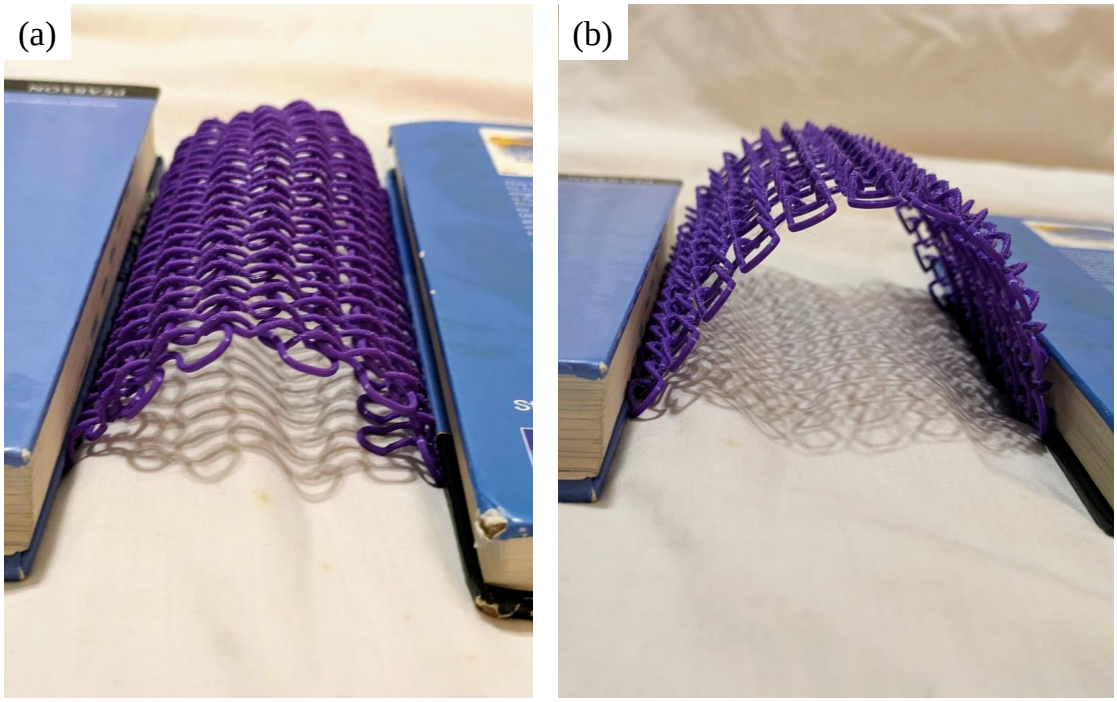

Figure 5.2: The self-actuating behavior of a base specimen when in compression from the (a) wale direction and (b) course direction

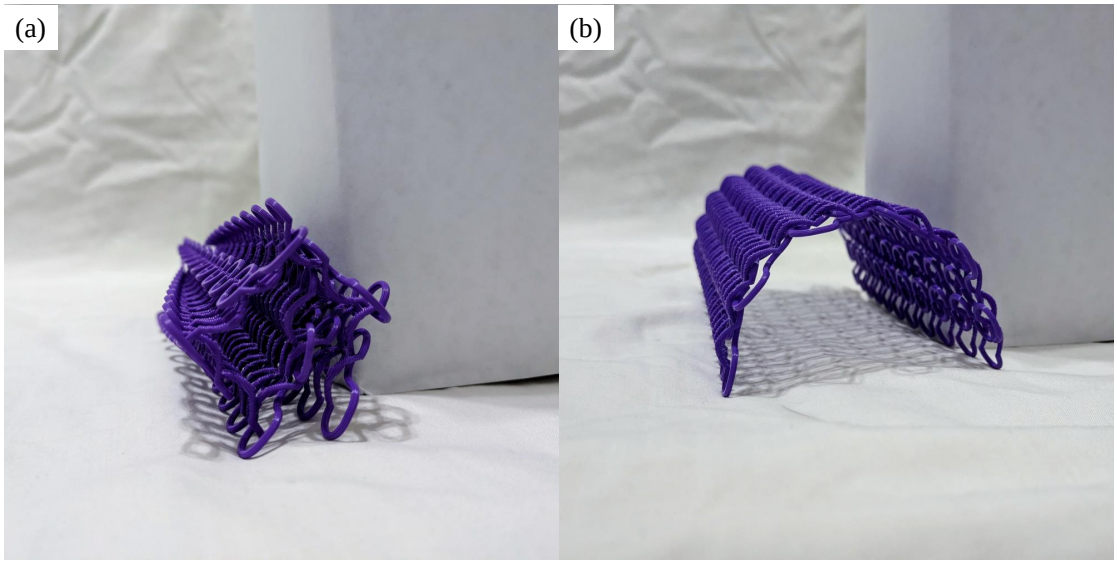

Figure 5.3: The behavior of the specimen when it is rolled in the (a) wale direction and (b) course direction

wale direction, the units take longer to "lock" together than they do when compression is applied in the course direction. Therefore, the course direction appears to require less force to create the domed shape. This also carries over to how the specimen can be transported. Fig. 5.3 shows the specimen rolled in the wale and course directions. Though it can be easily folded in the wale direction, similar to how it hung loose in Fig. 5.1, it will not roll in the course direction.

Another observation was that if a specimen is left in compression or tension for an extended amount of time, it forms to that shape. Some thermoplastics, such as PLA, have this malleable property, but fabric knitting also tends to be malleable. Some textile artists use it to prevent curling in a process called "blocking," but could it be also used to encourage the curling of a 3D printed knit?

Though these anisotropic properties can easily be qualitatively observed, the extent of them and quantitative information still needs to be studied.

Bibliography

C. Amanatides, O. Ghita, K. E. Evans, G. Dion, Characterizing and predicting the self-folding behavior of weft-knit fabrics, Textile Research Journal 92 (21-22) (2022) 4060–4076, doi:10.1177/00405175221099670.

M. Beecroft, 3D printing of weft knitted textile based structures by selective laser sintering of nylon powder, IOP Conference Series: Materials Science and Engineering 137 (1) (2016) 012017, doi:10.1088/1757-899X/137/1/012017.

M. Beecroft, Digital interlooping: 3D printing of weft-knitted textile-based tubular structures using selective laser sintering of nylon powder, International Journal of Fashion Design, Technology and Education 12 (2) (2019) 218–224, doi:10.1080/17543266.2019.1573269.

J. R. Campbell, Inkjet4Tex: Creative implications of 3D inkjet printing technologies for textiles, in: D. Durling, C. Rust, L. Chen, P. Ashton, K. Friedman (Eds.), Undisciplined! - DRS International Conference 2008, 16–19, URL https://dl.designresearchsociety.org/drs-conference-papers/drs2008/researchpapers/71/, 2008.

K. Chatterjee, T. K. Ghosh, 3D Printing of Textiles: Potential Roadmap to Printing with Fibers, Advanced Materials 32 (4) (2020) 1902086, doi:10.1002/adma.201902086.

S. Ding, B. Zou, P. Wang, C. Huang, J. Liu, L. Li, Geometric modeling and recycling of 3D printed fiber reinforced thermoplastic composite plain weft knitted structures, Composites Part A: Applied Science and Manufacturing 149 (2021) 106528, doi:10.1016/j.compositesa.2021.106528.

I. Gibson, D. W. Rosen, B. Stucker, Additive Manufacturing Technologies, Springer, 2020.

S. S. Gupta, Y. Y. Tan, P. Z. Chia, C. P. Pambudi, Y. H. Quek, C. Yogiaman, K. J. Tracy, Prototyping knit tensegrity shells: a design-to-fabrication workflow, SN Applied Sciences 2 (6) (2020) 1062, doi:10.1007/s42452-020-2693-4.

R. Kamien, Geometric Scaffolds for Knitting, in: Engineering Mechanics Insitute Conference, Baltimore, MD, 2022.

K. H. Leong, S. Ramakrishna, Z. M. Huang, G. Bibo, The potential of knitting for engineering composites—a review, Composites Part A: Applied Science and Manufacturing 31 (3) (2000) 197–220, doi:10.1016/S1359-835X(99)00067-6.

Y. Liu, L. Li, P. F. Yuan, A Computational Approach for Knitting 3D Composites Preforms, in: P. F. Yuan, Y. M. M. Xie, J. Yao, C. Yan (Eds.), Proceedings of the 2019 DigitalFUTURES, Springer Singapore, Singapore, 232–246, 2020.

R. Melnikova, A. Ehrmann, K. Finsterbusch, 3D printing of textile-based structures by Fused Deposition Modelling (FDM) with different polymer materials, IOP Conference Series: Materials Science and Engineering 62 (1) (2014) 012018, doi:10.1088/1757-899X/62/1/012018.

PolyMaker, Polylite PLA Technical Data Sheet, v5.0, 2018.

J. H. Porter, T. M. Cain, S. L. Fox, P. S. Harvey, Influence of infill properties on flexural rigidity of 3D-printed structural members, Virtual and Physical Prototyping 14 (2) (2019) 148–159, doi:10.1080/17452759.2018.1537064.

D. J. Spencer, Knitting Technology: A comprehensive handbook and practical guide, Woodhead Publishing, 3 edn., 2001.

J. Sun, W. Liao, Z. Yang, Additive Manufacturing of Liquid Crystal Elastomer Actuators Based on Knitting Technology, Advanced Materials 35 (36) (2023) 2302706, doi:10.1002/adma.202302706.

R. Uysal, J. Stubbs, A New Method of Printing Multi-Material Textiles by Fused Deposition Modelling (FDM), Tekstilec 4 (2019) 248–257, doi:10.14502/Tekstilec2019.62.248-257.

P. Wadekar, C. Amanatides, L. Kapllani, G. Dion, R. Kamien, D. E. Breen, Geometric modeling of complex knitting stitches using a bicontinuous surface and its offsets, Computer Aided Geometric Design 89 (2021) 102024, doi:10.1016/j.cagd.2021.102024.

P. Wadekar, P. Goel, C. Amanatides, G. Dion, R. D. Kamien, D. E. Breen, Geometric modeling of knitted fabrics using helicoid scaffolds, Journal of Engineered Fibers and Fabrics 15 (2020) 1558925020913871, doi:10.1177/1558925020913871.

S. Wickramasinghe, T. Do, P. Tran, FDM-Based 3D Printing of Polymer and Associated Composite: A Review on Mechanical Properties, Defects and Treatments, Polymers (Basel) 12 (7), doi:10.3390/polym12071529.

Y.-Q. Xiao, C.-W. Kan, Review on Development and Application of 3D-Printing Technology in Textile and Fashion Design, Coatings 12 (2) (2022) 267, doi:10.3390/coatings12020267.

Appendix A

Print Settings

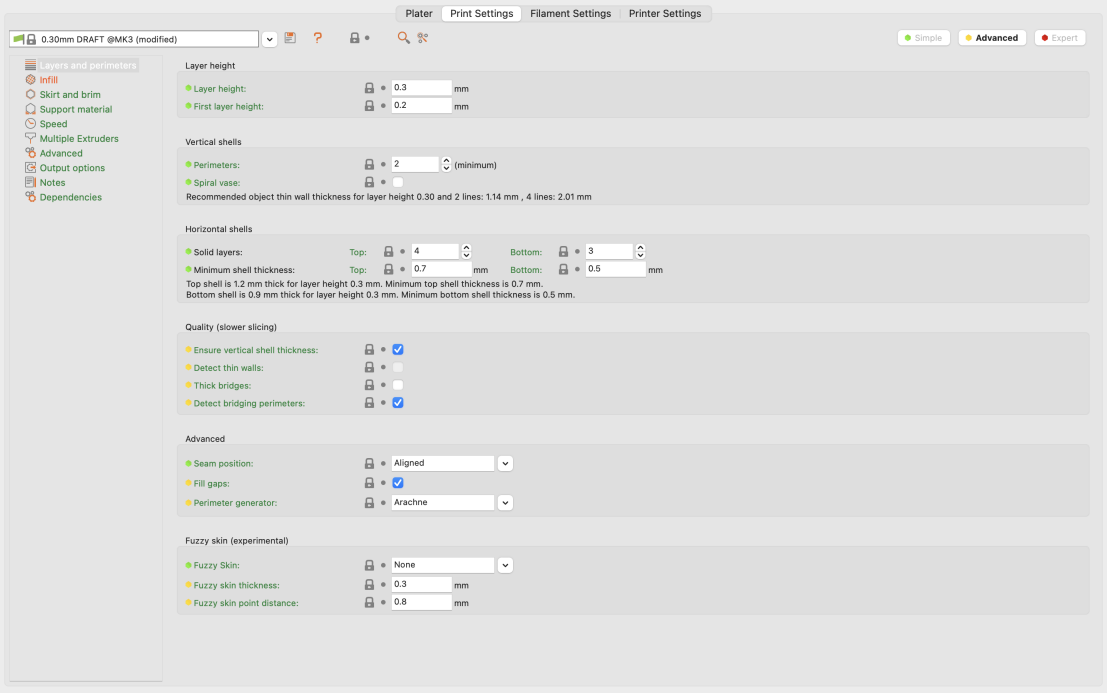

Figure A.1: Layer Settings

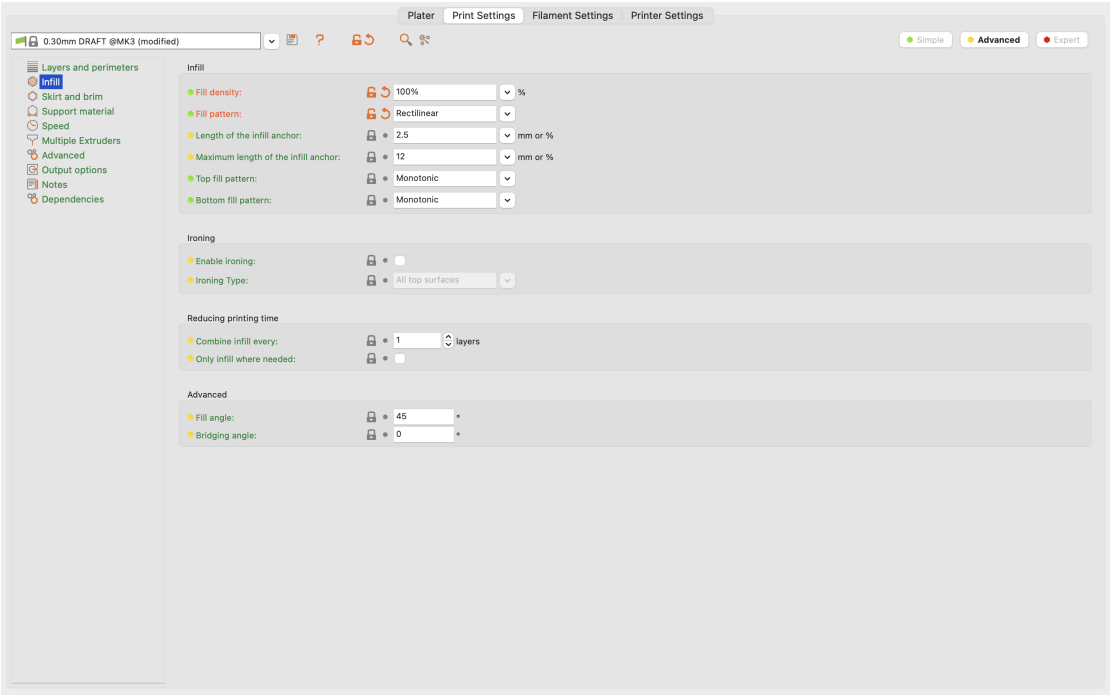

Figure A.2: Infill Settings

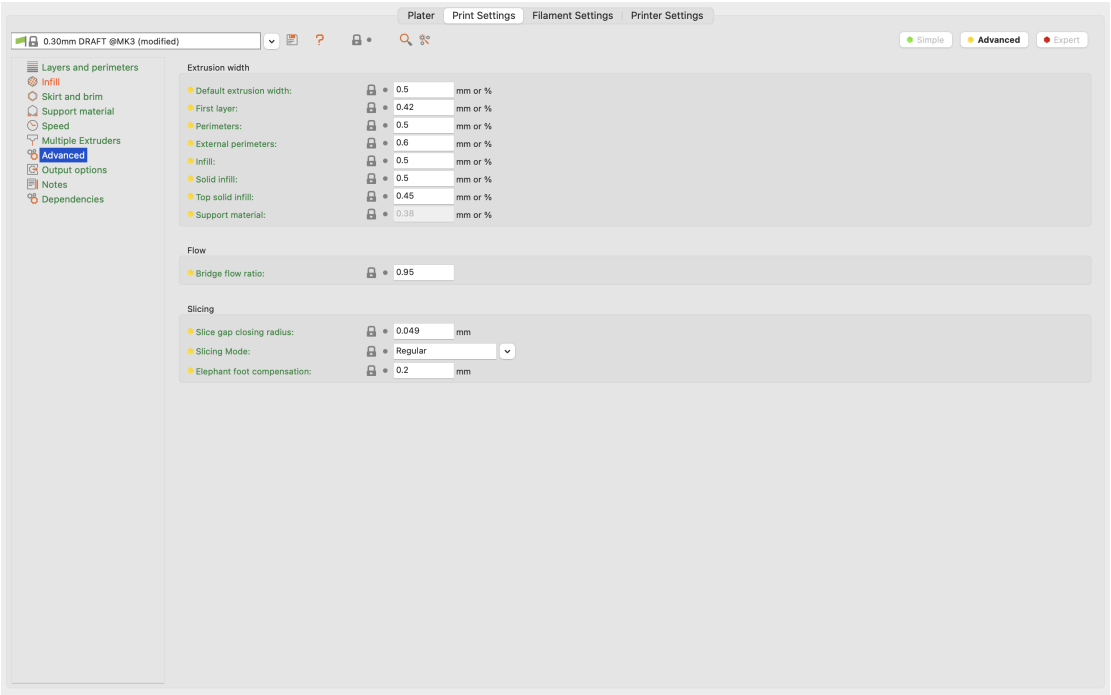

Figure A.3: Advanced Settings

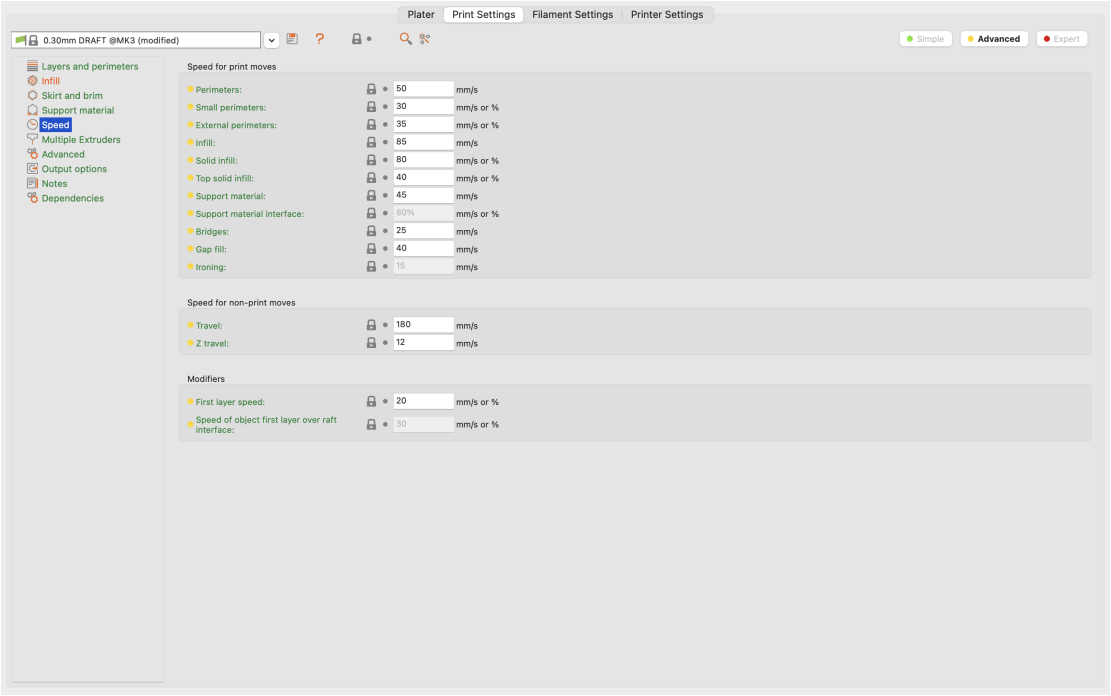

Figure A.4: Speed Settings